TECHNICAL NOTE

D-1692

A THEORY AND APPLICATIONS OF FILAMENTARY STRUCTURES

By H. U. Schuerch, O. R. Burggraf, and A. C. Kyser

NATIONAL AERONAUTICS AND SPACE ADMINISTRATION

WASHINGTON   December 1962

NATIONAL AERONAUTICS AND SPACE ADMINISTRATION

TECHNICAL NOTE D-1692

A THEORY AND APPLICATIONS OF

FILAMENTARY STRUCTURES

By H. U. Schuerch, O. R. Burggraf,
and A. C. Kyser

Astro Research Corporation
Santa Barbara, California

SUMMARY

A theory of filamentary structures consisting of monotropic membranes is presented. Applications to isotensoid pressure vessels with rotational symmetry demonstrate the use of the theory. Particular attention is given to applications of filamentary design of variable-geometry expandable structures.

An extension of the theory to pressurized filamentary structures subject to centrifugal loading and the special case of meridional winding patterns are presented in two Appendices.

Physical interpretation of the resulting shapes and winding patterns leads to a discussion of the morphology of filament-wound pressure vessels.

Experimental data, obtained from filament-wound toroidal pressure vessels, confirm the validity of the theory and demonstrate application of the analytical design technique for filamentary structures.

INTRODUCTION

A review of recent developments in the field of advanced structures for aeronautical, missile-borne, and space applications shows an increasing interest in exploiting the remarkable physical-mechanical properties of fibered materials. A large volume of published information (See, for instance, references 1, 2, 3, and 4) is available, particularly in the field of filament wound structures. The attraction of filamentary structures may be found in three areas:

(1) Structures of considerably higher strength/weight ratios are potentially possible (and have, in certain instances, been demonstrated) by use of filamentary materials as compared to similar structures made from conventional isotropic material (reference 5).

(2) The potential of obtaining relative insensitivity to crack-propagation due to accidental damage in filamentary arrays typical for filament-wound structures has been shown theoretically by Hedgepeth (reference 6). Furthermore, tests on single fibers of many materials show increased strength and resistance to elevated temperature (reference 7), creep, and fatigue as compared to the properties of the same materials in bulk form. Realization of the implied potential performance gains depends upon proper utilization of fibers (isotensoid design) and remains to be generally demonstrated in practice.

(3) The peculiar, non-isotropic character of the filamentary textured material may be used to advantage in specific applications. One of particular interest is the design of expandable structures with variable geometry, for which a multitude of space applications are presently considered. A general analytical treatment of the problem of large deformations in elastic materials reinforced by inextensible chords has been presented in reference 8.

There exists a need for a fundamental approach to the problem of design synthesis of filamentary structures. The present report deals with a specific and relatively important species of filamentary structures, namely those produced by filament-winding processes, both from the point of view of developing a basic understanding, and

from the point of view of particular applications to toroidal pressure containers.

This investigation was performed with the financial assistance of the National Aeronautics and Space Administration under Contract NASr-8.

SYMBOLS

C	Fiber helix parameter
EI	Bending stiffness of analog column
$E_I G_I$	Coefficients of the first fundamental form
$E_{II} G_{II}$	Coefficients of the second fundamental form
$\mathcal{E}$	Elliptical integral of the second kind
F	Force/unit length
$\mathfrak{F}$	Elliptical integral of the first kind
K	Pressure load parameter
N_i	Fraction of filament count
P	Load, (also used as "point on surface")
R	Non-dimensional radial coordinate
T	Fiber force
V	Volume
$\overline{X}$	Radius vector
Z	Non-dimensional axial coordinate
$\overline{e}$	Unit vector

4

h	Distance between poles
i	Integer
k	Curvature
$\hbar$	Argument of elliptical integral
ℓ	Specific strength
n	Number of filaments (fiber count)
m'	Mass/unit length
p	Pressure
r	Radius
s	Arc length
u, v	Curvilinear coordinates
x y z	Cartesian coordinates
Ω	Centrifugal load parameter
α	Slope of meridian
β	Helix angle
δ	Central angle of fiber spacing
φ	Central angle
ρ	Radius of curvature
ω	Angular velocity
ξ	Integration variable

THEORY OF MONOTROPIC MEMBRANES

Definitions

Consider a thin-walled shell made from a material which consists of an array of filaments as shown in figure 1. The thickness of the shell may be variable, but will always be sufficiently small so that the geometrical properties of the shell can be described by its middle surface (membrane).

Consider now a small but finite domain of this shell. The geometrical arrangement of the filaments traversing this domain shall be such that the tangents to all filaments have a uniquely determined direction, described by an angle β between the filament centerlines and a coordinate line inscribed on the membrane surface. The centerlines of all filaments, thus, belong to a "one parametric" family of curves. Mathematically, this can be expressed by

$$\beta = \beta_{(u, v)} \tag{1}$$

where u and v are surface coordinates and $\beta_{(u, v)}$ is a unique and continuous function of the surface coordinates u and v. The condition of uniquely defined filament direction shall hold for all regular points of the membrane, but may not hold for points of singularity such as poles, lines of cross-over, etc.

Assume that the filaments are completely flexible and capable of carrying only normal forces only in the direction β of their local tangents. If these filaments are bonded together by a matrix material, consider this matrix to be completely compliant such that stresses in the matrix are negligible. Thus, the only stresses that can exist in this shell are normal stresses in the locally defined direction β .

A structure of this nature shall be called a Monotropic Membrane, to indicate the unique and predetermined character of stress distribution.

Filament-wound structures can frequently be considered as combinations of contiguous or intermeshing monotropic membranes.

This is particularly true if the filaments are relatively rigid and the matrix or binder material is relatively flexible, so that the predominant part of the structural loading is carried by the filamentary constituent of the composite material.

Geometry of Monotropic Membranes

In this paragraph, geometrical relations referring to surfaces and curves on surfaces are summarized from references 9 through 11 for convenience of the subsequent discussion of the properties of monotropic membranes.

Consider the middle surface of the shell described by a vector $\bar{X}$ extending from an arbitrary origin "O" to any point "P" on the surface shown in figure 2. The surface is inscribed with a system of orthogonal curvilinear coordinates u, v . For the purpose of this discussion, the lines $u = $ Constant and $v = $ Constant will be chosen as the lines of principal curvature of the surface.

Let $(\bar{e}_t, \bar{e}_n, \bar{e}_g)$ be a triad of mutually orthogonal unit vectors, moving along the centerline of a filament located on the surface where

$\bar{e}_t$ is tangential to the filament centerline

$\bar{e}_n$ is perpendicular to the surface

$\bar{e}_g$ is located in the tangent plane to the surface centerline and normal to the filament tangent.

The rate of change of the unit tangent vector $\bar{e}_t$, while proceeding along the filament centerline for a differential length ds , is equal to the curvature vector:

$$\bar{k} = \frac{d\bar{e}_t}{ds} \qquad (2)$$

where $\bar{k}$ is a vector collinear with the radius vector of curvature $\bar{\rho}$ and of absolute magnitude $\frac{1}{\rho}$.

The <u>normal curvature vector</u> $\bar{k}_n$ is the projection of $\bar{k}$ into a plane spanned by $\bar{e}_t$ and $\bar{e}_n$. Its magnitude, the <u>normal curvature</u>, can be expressed by the scalar vector product

$$k_n = (\bar{k} \cdot \bar{e}_n) \tag{3}$$

The <u>geodesic curvature vector</u> $\bar{k}_g$ is the projection of $\bar{k}$ into the tangent plane to the surface. Its magnitude, the <u>geodesic curvature</u>, can be expressed by the scalar vector product

$$k_g = (\bar{k} \cdot \bar{e}_g) \tag{4}$$

Curves of vanishing geodesic curvature are called <u>geodesics</u>. They have the characteristics of straight lines in the non-Euclidian geometry of the surface described by $\bar{X}$. Thus, they are also curves of minimum (or maximum) distance between two points on the surface. A particularly important characteristic of geodesics is the fact that geodesics retain their geodesic character during an inextensional (bending) deformation of the membrane.

The pertinent geometrical properties of the surface can be expressed in terms of two fundamental quadratic forms:

(1) The <u>first fundamental form</u> describes the length ds of a line element on the surface. For an orthogonal surface coordinate system (u, v) this first fundamental form reduces to

$$(ds)^2 = (d\bar{X} \cdot d\bar{X}) = E_I du^2 + G_I dv^2 \tag{5}$$

where

$$E_I = \left(\frac{\partial \bar{X}}{\partial u} \cdot \frac{\partial \bar{X}}{\partial u} \right.$$

$$G_I = \left. \frac{\partial \bar{X}}{\partial v} \cdot \frac{\partial \bar{X}}{\partial v} \right)$$

(2) The <u>second fundamental form</u> is a measure of the change of the surface tangent plane or surface normal vector, i. e. , a

8

measure for the curvature and twist of the surface. For orthogonal coordinate systems, the second fundamental form reduces to

$$- (d\overline{X} \cdot d\overline{e}_n) = E_{II}du^2 + G_{II}dv^2 \tag{6}$$

where

$$E_{II} = \left(\frac{\partial^2 \overline{X}}{\partial u^2} \cdot \overline{e}_n \right.$$

$$G_{II} = \left. \frac{\partial^2 \overline{X}}{\partial v^2} \cdot \overline{e}_n \right)$$

Now let $k_{n(v)}$ and $k_{g(v)}$ be the normal and geodesic curvature of the lines $v = $ Constant , and let $k_{n(u)}$ and $k_{g(u)}$ be the normal and geodesic curvature of the lines $u = $ Constant .

The normal curvature of the filament centerline forming an angle β with the line $v = $ Constant is then given by Euler's Theorem for the orthogonal system of surface coordinates formed by the lines of principal curvature:

$$k_{n(\beta)} = k_{n(v)} \cos^2\beta + k_{n(u)} \sin^2\beta \tag{7}$$

The geodesic curvature of the filament centerline forming an angle β with the line $v = $ Constant is given by Liouville's Theorem for any orthogonal system of surface coordinates:

$$k_{g(\beta)} = \frac{d\beta}{ds} + k_{g(v)} \cos\beta + k_{g(u)} \sin\beta \tag{8}$$

Finally, the normal and geodesic curvatures of the coordinate lines are related to the coefficients of the first and second fundamental forms of equations (5) and (6) as follows:

$$\left. \begin{array}{l} k_{n(v)} = \dfrac{E_{II}}{E_I} \\[3mm] k_{n(u)} = \dfrac{G_{II}}{G_I} \end{array} \right\} \tag{9}$$

$$k_{g(v)} = - \frac{\partial E_I}{\partial v} \frac{1}{2E_I \sqrt{G_I}}$$

$$k_{g(u)} = \frac{\partial G_I}{\partial u} \frac{1}{2G_I \sqrt{E_I}}$$

(10)

Equilibrium Condition

Consider an element of a filament of length ds , subject to an axial force vector $\overline{T}$ and an external force vector/unit length F' of arbitrary direction as shown in figure 3. Equilibrium for the element demands that

$$\overline{T}_{(s+ds)} - \overline{T}_{(s)} + \overline{F}'_{(s)} \, ds = 0$$

or, in differential vector form

$$\frac{d\overline{T}_{(s)}}{ds} + \overline{F}'_s = 0 \tag{11}$$

The vector $\overline{T}_{(s)}$ can be written as $\overline{T}_{(s)} = \overline{e}_t \cdot T_{(s)}$, where $T_{(s)}$ is the magnitude of the force vector $\overline{T}$ at s . Thus, equation (11) can be written as

$$\frac{d}{ds} (T_{(s)} \cdot \overline{e}_t) + \overline{F}' = 0$$

and by partial differentiation of the first term, considering equation (2) yields:

$$\frac{dT_{(s)}}{ds} \overline{e}_t + T_{(s)} \overline{k} + \overline{F}'_{(s)} = 0 \tag{12}$$

Scalar multiplication of equation (12) in turn with the three unit vectors of the triad $(\overline{e}_t, \overline{e}_n, \overline{e}_g)$ yields three scalar equilibrium conditions:

$$\frac{dT}{ds} + F'_t = 0 \tag{13}$$

$$Tk_n + F'_n = 0 \tag{14}$$

$$Tk_g + F'_g = 0 \tag{15}$$

where

$$F'_t = (\overline{F}' \cdot \overline{e}_t)$$

$$F'_n = (\overline{F}' \cdot \overline{e}_n)$$

$$F'_g = (\overline{F}' \cdot \overline{e}_g)$$

are the three components of the external load vector in the three directions indicated by the triad $(\overline{e}_t, \overline{e}_n, \overline{e}_g)$, respectively (figure 3).

Discussion

The equations (13) through (15) relate the filament load to the geometrical characteristics of the filament given by $\overline{e}_t$, k_n , and k_g . The two curvatures are related to the properties of the lines of principal curvature serving as surface coordinates by Euler's and Liouville's Theorems, equations (7) and (8) respectively, and may be related to the coefficients of the fundamental forms as given in equations (9) and (10).

An examination of the equilibrium equations (13) through (15) yields the following results:

(1) For a given monotropic shell, only one of the three components of external load vector $\overline{F}'$ can be freely chosen, while still satisfying all conditions of equilibrium. This implies that the monotropic shell is twofold statically underdeterminate, i. e. , it will act as a mechanism rather than as a structure under all external loads not satisfying the conditions of equations (13) through (15). This effect may be beneficial where a

"variable geometry structure" such as a foldable and expandable shell is desired. On the other hand, however, peculiar instability phenomena, as discussed in the latter portion of this report, may occur, requiring particular study and attention.

In general, it is necessary to have three contiguous or intermeshing layers of monotropic membranes present in a structural shell in order to produce a statically determinate system.

(2) For the case where $F'_t = 0$, the fiber force T is invariant throughout the structure. Such a structure is called "Isotensoid" (from iso-equal, tensus-extension) to indicate the uniform character of stress and strain in the load carrying material. An isotensoid structure, furthermore, constitutes an optimum design, since the material will be stressed equally (i. e. , utilized uniformly) at all points.

(3) For monotropic shells that are loaded by pressure loads normal to the surface, both F'_t and F'_g vanish. The structure is isotensoid and the geodesic curvature k_g of the filaments vanishes; therefore, the curves of filament centerlines describe geodesics of the membrane surface. These are of particular importance for the case of filament winding, since a fiber placed under some tension on an arbitrarily shaped mandrel will tend to follow a geodesic on the mandrel surface.

The general problem of optimum isotensoid design synthesis for a filament-wound structure may now be stated as follows:

For a given external load, find the surface shape and associated filamentary geometry of one or several monotropic membranes for which F'_t vanishes.

This problem, applied to pressure loaded shells of revolution, will be discussed in detail in the remaining portion of the report. A different situation arising from a combination of pressure and centrifugal loads is discussed in Appendix A. This case demonstrates the application of the basic approach to filamentary design of not necessarily isotensoid character and for more complex loading conditions.

ISOTENSOID PRESSURE SHELLS OF REVOLUTION

Basic Equations

Consider a surface of revolution (r, φ, z) , as shown in figure 4. The coordinates of the vector $\overline{X}$ extending from the origin of a Cartesian system (x y z) are

$$\overline{X} = \begin{pmatrix} r \ \cos\varphi \\ r \ \sin\varphi \\ z \end{pmatrix} \tag{16}$$

The lines of principal curvature used as surface coordinate lines are the parallel circles $u = z = $ Constant and the meridians $v = \varphi = $ Constant .

The differential vector $d\overline{X}$ in terms of the coordinates $(z\varphi)$, is:

$$d\overline{X} = \frac{\partial \overline{X}}{\partial z} dz + \frac{\partial \overline{X}}{\partial \varphi} d\varphi = \begin{pmatrix} \dfrac{dr}{dz} \cos\varphi \ dz - r \ \sin\varphi \ d\varphi \\ \dfrac{dr}{dz} \sin\varphi \ dz + r \ \cos\varphi \ d\varphi \\ dz \end{pmatrix} \tag{17}$$

The unit vector normal to the surface has the coordinates

$$\overline{e}_n = \begin{pmatrix} \cos\alpha \ \cos\varphi \\ \cos\alpha \ \sin\varphi \\ \sin\alpha \end{pmatrix} \tag{18}$$

where α is the angle between the local surface normal $\overline{e}_n$ and the (x y) plane.

The second derivatives of $\overline{X}$, with respect to the principal curvature coordinates, are:

$$\frac{\partial^2 \overline{X}}{\partial z^2} = \begin{pmatrix} \dfrac{d^2 r}{dz^2} \cos\varphi \\[2ex] \dfrac{d^2 r}{dz^2} \sin\varphi \\[2ex] 0 \end{pmatrix}$$

and

$$\frac{\partial^2 \overline{X}}{\partial \varphi^2} = \begin{pmatrix} -\, r \, \cos\varphi \\[1ex] -\, r \, \sin\varphi \\[1ex] 0 \end{pmatrix}$$

$$(19)$$

From equations (5) and (17) the coefficients of the first fundamental form become:

$$E_I = \left(\frac{\partial \overline{X}}{\partial z} \cdot \frac{\partial \overline{X}}{\partial z} \right) = 1 + \left(\frac{dr}{dz} \right)^2$$

$$G_I = \left(\frac{\partial \overline{X}}{\partial \varphi} \cdot \frac{\partial \overline{X}}{\partial \varphi} \right) = r^2$$

$$(20)$$

Similarly, from equations (6), (18), and (19) the coefficients of the second fundamental form become:

$$E_{II} = \left(\frac{\partial^2 \overline{X}}{\partial z^2} \cdot \overline{e}_n \right) = \frac{d^2 r}{dz^2} \cos\alpha$$

$$G_{II} = \left(\frac{\partial^2 \overline{X}}{\partial \varphi^2} \cdot \overline{e}_n \right) = -\, r \, \cos\alpha$$

$$(21)$$

From equations (20) and (21) the principal curvatures of the coordinate lines become:

14

$$k_{n(v)} = \frac{E_{II}}{E_I} = \frac{\dfrac{d^2 r}{dz^2}}{\left(1 + \left(\dfrac{dr}{dz}\right)^2\right)^{3/2}} = -\frac{1}{\rho_M} \qquad (22)$$

$$k_{n(u)} = \frac{G_{II}}{G_I} = -\frac{\cos\alpha}{r} \qquad (23)$$

The negative signs appearing in equations (22) and (23) are a consequence of the sign conventions used for α and ρ_M , as indicated in figure 4. It is, of course, possible to derive the values of principal curvature by inspection of figure 4 directly. The analytical development has been given here to demonstrate the application of an approach that may be used for analysis of generalized surfaces.

The normal curvature in direction β becomes, according to Euler's Theorem (equation (7)):

$$k_{n\beta} = -\frac{1}{\rho_M} \cos^2\beta - \frac{\cos\alpha}{r} \sin^2\beta \qquad (24)$$

The direction β of the geodesic filament is obtained by integration of Liouville's Theorem (equation (8)) with $k_{g(\beta)} = 0$. For surfaces of revolution, this integration yields the Theorem of Clairaut:

$$\sin\beta = \sin\beta_o \frac{r_o}{r} \qquad (25)$$

where $\sin\beta_o$ and r_o are arbitrary constants of integration.

Let $\qquad C = \sin\beta_o$: filament helix parameter characteristic for the filamentary geometry.

$\qquad\quad R = r/r_o$: non-dimensional radius of shell.

Then, equation (25) can be written as

$$\sin\beta = \frac{C}{R} \tag{25a}$$

and

$$\cos\beta = \frac{1}{R}\sqrt{R^2 - C^2} \tag{25b}$$

Consider now a structural shell of revolution consisting of several layers of monotropic membranes, as shown in figure 5, subject to a rotationally symmetrical pressure load $p_{(z)}$ that may be variable along the meridian, but is uniform along any parallel circle. Each monotropic membrane is assumed to comprise n_i filaments uniformly spaced along any parallel circle of the shell, each filament of each monotropic membrane forming an angle $\sin\beta_{o_i} = C_i$ with the meridian at the extreme perimeter of radius r_o, and each filament carrying an equal and uniform axial force T.

The normal load/unit length carried by each filament is

$$F'_{n_i} = p_i \frac{2r\pi}{n_i} \cos\beta_i \tag{26}$$

where p_i is the normal pressure carried by each monotropic membrane "i" .

The equilibrium condition (equation (14)), considering equations (26) and (24), then becomes

$$-\frac{1}{\rho_M}\cos\beta_i - \frac{\cos\alpha}{r}\frac{\sin^2\beta_i}{\cos\beta_i} + p_i\frac{2r\pi}{n_i T} = 0 \tag{27}$$

introducing the "non-dimensional" filament count $N_i = \frac{n_i}{n}$, where n is the total number of filaments traversing a parallel circle, and substituting equations (25a) and (25b) into equation (27) yields:

$$p_i = \frac{nT}{2\pi r_o^2 R}\left\{\frac{N_i C_i^2 \cos\alpha}{R^2\sqrt{R^2 - C_i^2}} + \frac{r_o}{\rho_M}\frac{N_i\sqrt{R^2 - C_i^2}}{R}\right\} \tag{28}$$

16

Summing over all monotropic membranes "i" , and solving for the non-dimensional meridional curvature yields:

$$\frac{r_o}{\rho_M} = \frac{-1}{\sum N_i \sqrt{R^2 - C_i^2}} \left\{ \frac{\cos\alpha}{R} \sum \frac{N_i C_i^2}{\sqrt{R^2 - C_i^2}} - KR^2 \frac{P_{(z)}}{P_o} \right\} \quad (29)$$

where $K = \dfrac{2\pi p_o r_o^2}{nT}$ is the non-dimensional pressure load parameter which is characteristic for the curvature properties of the shell.

Equation (29) describes the meridional curve of the shell of revolution in terms of the intrinsic coordinates ρ_M and α , as a function of the characteristic parameters C_i and K .

An integral form of equation (29) can be derived by considering the equilibrium conditions pertaining to the whole shell, as shown in figure 5.

Equilibrium in axial direction requires:

$$\left(\sum N_i \, nT \, \cos\beta_{o_i} \right) - r_o^2 \pi p_o = \left(\sum N_i \, nT \, \cos\alpha \, \cos\beta_i \right) - R^2 r_o^2 \pi p_{(z)}$$

or, solved for $\cos\alpha$:

$$\cos\alpha = \frac{R}{\sum N_i \sqrt{R^2 - C_i^2}} \left\{ \left(\sum N_i \sqrt{1 - C_i^2} \right) - \frac{K}{2} \left(1 - R^2 \frac{P_{(z)}}{P_o} \right) \right\} \quad (30)$$

Equilibrium in torque around the z-axis for a single filament requires (since the pressure loading can not contribute to a torque):

$$T \sin\beta_i \, r = T \sin\beta_{o_i} \, r_o$$

which simply reduces to the Theorem of Clairaut (equation (25)) by division through T.

For the complete shell, torsional equilibrium in absence of an externally applied torque requires:

$$\Sigma \, N_i \, C_i \;=\; 0 \qquad\qquad (31)$$

A further condition is imposed for closed pressure vessels of singly connected volume without externally applied axial forces ("Bottles").

For this case, axial equilibrium requires that:

$$\Sigma \, N_i \, \sqrt{1 - C_i} \;=\; \frac{K}{2} \qquad\qquad (32)$$

Finally, the problem of defining the filamentary geometry can be solved by integration of the differential geometrical relationship between φ and α, along a geodesic. By inspection of figure 4 we obtain:

$$\rho_M \, d\alpha \, \tan\beta \;=\; r \, d\varphi$$

or, integrated

$$\varphi_{(\alpha)} \;-\; \varphi_{(\alpha=0)} \;=\; \int_0^\alpha \frac{C_i}{R\sqrt{R^2 - C_i^2}} \, \frac{\rho_M}{r_o} \, d\xi \qquad\qquad (33)$$

Methods of Solution

Equation (30) represents an integral form of equation (29) which can be transformed into a first-order non-linear differential equation for $R_{(Z)}$ suitable for numerical integration by substituting

$$\cos\alpha \;=\; \frac{-1}{\sqrt{1 + \left(\dfrac{dR}{dZ}\right)^2}}$$

where $Z = \dfrac{z}{r_o}$ is the non-dimensionalized axial coordinate.

The resulting differential equation can be written in finite difference form for numerical integration by means of a digital computer.

A program has been prepared for an IBM, Type 1620 computer, capable of handling arbitrary inputs for N_i, C_i and K , and computing both intrinsic $(\rho,\ \alpha)$ and non-dimensionalized Cartesian coordinates (R, Z) of the meridional shapes by means of a modified Runge-Kutta method (reference 12). Additional output data available from the program are the filament geometry $\varphi_{(\alpha)}$ as well as surfaces S and enclosed volumes V of the bodies of revolution generated by rotating the meridional curves (R, Z) around the z-axis.

Analytical solutions of equation (30) are possible. These lead to expressions which may be reduced to elliptical integrals. In the general case, however, the resulting expressions are quite involved and time-consuming for evaluation. As a consequence, direct digital integration appears to be a more economical approach for the purpose of obtaining design data. An exception is the case for C = 0 , discussed in Appendix B. There, the solution can be reduced to simple combinations of elliptical integrals of the first and second kind, which are tabulated, for instance, in reference 13.

For the purpose of a graphical solution, equations (29) and (30) are suitable in their intrinsic form. Tables of ρ_M and α in function of r/r_o can be computed for any given set of K, C_i, N_i from equations (30) and (29). With slope α and radius of curvature ρ_M known, very accurate meridional shapes can be constructed by means of rule, compass, and protractor.

In addition to the numerical and graphical methods mentioned, the particular case of C = 0 (i.e., meridional fiber direction only) allows solution of the isotensoid meridional shape equations by means of a column analog, as shown in figures 6 and 7. This analog is described in more detail in Appendix B.

All three methods, digital integration, graphical solution, and column analogy, have been used to generate the data shown in figures 10 through 20 of this Technical Note.

Discussion of Results

For the purpose of an initial evaluation of possible isotensoid pressure vessels, the number of free parameters may be reduced as follows:

(1) The pressure p is assumed to be constant throughout the length of the shell, i. e., $p_{(z)} = p_o$ = Constant.

(2) The shells are considered to consist of two monotropic membranes satisfying the torque equilibrium equation (31):

where $N_1 = N_2 = 0.5$

and $C_1 = - C_2 = C$

With these assumptions, the intrinsic equations (29) and (30) reduce to

$$\frac{r_o}{\rho_M} = \frac{-1}{\sqrt{R^2 - C^2}} \left\{ \frac{\cos\alpha}{R} \frac{C^2}{\sqrt{R^2 - C^2}} - K R^2 \right\} \quad (29b)$$

and, in integral form:

$$\cos\alpha = \frac{R}{\sqrt{R^2 - C^2}} \left\{ \sqrt{1 - C^2} - \frac{K}{2} \left(1 - R^2 \right) \right\} \quad (30b)$$

where C and K are the defining parameters of the isotensoid pressure shell.

Inspection of equations (29b) and (30b) shows that no real solutions for either ρ or α exist if R < C . Thus, the minimum distance from the axis of rotation which a geodesic filament can have is given by its helix angle defined by C . An important design implication that may be derived from this is that there will always be a polar opening for any geodesically helix wound (C ≠ 0) pressure vessel. The size of the polar opening R_{min} can be computed from equation (30b) by letting

$$\cos\alpha = \pm 1$$

Excluding the trivial solution $R = 1$, a relation between K, C, and R_{min} is obtained:

$$\frac{K}{2} \left(1 - R^2_{min}\right) = \pm \left\{ \frac{\sqrt{R^2_{min} - C^2}}{R_{min}} + \sqrt{1 - C^2} \right\} \quad (34)$$

This equation is useful if R_{min} is given as a design parameter, and a compatible pair C and K need to be determined for the design of the pressure vessel.

The solutions that may be obtained for the meridional shapes $R_{(Z)}$ by solution of the intrinsic equations (29b) and (30b) can be classified according to their general character for a range of parameter K .

For the purpose of this discussion, only the range of $K \geq 0$ will be considered. Negative K-values yield similar shapes (corresponding to either negative pressure or compressive fiber force) and yield no new general insight into the problem even though they may be important for particular design objectives. The various shapes for positive K-values are discussed below and are shown in schematic form in figures 8 and 9:

(1)   Hyperboloid (figure 8(a))

Here the extreme perimeter r_o is a minimum. For all positive z , $\cos\alpha$ is always negative and ρ_M is always positive. This requires $K = 0$ and results in the filaments being straight lines rotating around the z-axis , forming a hyperboloid of revolution. This is a surface of zero curvature, corresponding to zero internal pressure p .

(2)   Cylinder (figure 8(b))

For a cylinder $R \equiv 1$, $\cos\alpha \equiv 0$ and $\rho_M = \infty$. These conditions are satisfied if

$$K = \frac{C^2}{\sqrt{1 - C^2}}$$

(3) Corrugated Tube (figure 8(c))

A corrugated tube will exhibit a point of inflection where $\rho_M = \pm \infty$ at a value of $R > C$. α will always be smaller than $\pm \dfrac{\pi}{2}$. This requires that

$$0 < K < \frac{2}{\sqrt{1 - C^2}}$$

If $K < \dfrac{C^2}{\sqrt{1 - C^2}}$, then the corrugations are located outside the cylinder $R = 1$ and r_o is a minimum; if

$K > \dfrac{C^2}{\sqrt{1 - C^2}}$, then the corrugations are inside the cylinder $R = 1$, and r_o is a maximum, as indicated in figure 8(c).

For those corrugated tubes ("bottles") which satisfy the axial equilibrium equation (32), the following relations hold:

The minimum radius R_{min} is related to the fiber helix parameter C by

$$\sqrt{1 - C^2} = \frac{\sqrt{R_{min}^2 - C^2}}{R_{min}^3}$$

The slope α of the meridian is given by

$$\cos\alpha = R^3 \sqrt{\frac{1 - C^2}{R^2 - C^2}}$$

The radius at the inflection point of the meridian is

$$R_{(\rho = \infty)} = \sqrt{3/2}\ C$$

The slope at the inflection point is given by

$$\cos\alpha_{(\rho=\infty)} = \frac{3}{2} \sqrt{3} \; c^2 \sqrt{1 - c^2}$$

(4) Cusp (figure 8(d))

For the case of a cusp, the angle α becomes indefinite and ρ_M becomes 0 at $R = C$. This condition is satisfied if

$$K = \frac{2}{\sqrt{1 - c^2}}$$

The cusp shape constitutes the transition between the corrugated tube and the progressive loop.

(5) Loop (figure 9)

Looped curves, which are of particular interest for the generation of toroidal pressure vessels, are generated if ρ_M is negative for all values of R . This requires

$$K > \frac{2}{\sqrt{1 - c^2}}$$

Three distinct types of loops are generated as K increases:

(a) A progressive, periodic loop (figure 9(a)).

(b) A closed loop forming the transition between progressive and regressive, periodic loops (figure 9(b)).

(c) A regressive, periodic loop (figure 9(c)).

The radius R_H at which the meridional curve is horizontal (i. e., the location of maximum thickness of the toroid generated by rotation of the loop) is

$$R_{(\alpha=\pi/2)} = \sqrt{1 - \frac{2}{K}} \sqrt{1 - c^2}$$

A summary of the domains in the positive K-C plane corresponding to the various types of solutions is shown in figure 10. Also shown in figure 10 are the curves R_{min} = Constant , and the C-K values resulting in "bottles" according to equation (32).

A number of cases for various parameter combinations have been worked out by digital integration of equations (30) and (33) complemented by graphical and column analog studies. Primary attention was given to the looped type of solutions which are of interest in the design of toroidal pressure vessels.

Figures 11 through 14 show the meridional shapes for 1/2 period $(0 \leqq \alpha \leqq \pi)$ of double helix wound shells according to equations (29b) and (30b) for $K \geqq \dfrac{2}{\sqrt{1 - C^2}}$ and for C-values of 0, .25, .5, and .75, respectively.

Figures 15 through 17 show solutions for the case of looped meridians for shells consisting of three layers; $C_1 = 0$, $C_2 = .5$, and $C_3 = -.5$, with variable ratios of N_1/N_2 and with $N_2 = N_3$.

Figure 18 shows a case with 6 layers, representing the case of a corrugated tube, together with the filamentary geometry of the various layers.

In the cases of multiple C-values, shown in figures 15 through 18, return points occur at $R = C_i$, where the corresponding monotropic membrane folds back into itself, reversing the helix angle and thus forming $C_{i+1} = -C_i$.

Figure 19 shows an example of an unsymmetrical loop resulting from linearly variable pressure simulating the situation of a pressure vessel subject to hydrostatic pressure gradients such as may be encountered in a liquid container during the boost phase of a rocket.

Figure 20 shows a realization of the particular case for a closed loop indicating the general shape and the disposition of the winding pattern.

MORPHOLOGY OF CLOSED PRESSURE VESSELS

The range of possible isotensoid pressure shells of revolution with meridional shapes, as shown in figures 11 through 20, is limited by the restriction of the parameter ranges and combinations that have been considered. Nevertheless, five basic types of possible closed pressure vessel designs are identifiable from a review of the presented material. A brief discussion of their general characteristics follows:

Containers with Simply Connected Volume

(1) Type 1 (figure 21): Closed shells containing a monotropic membrane with meridional fiber direction (C = 0) crossing the z-axis .

In the special case where the "bottle" relationship of K and C_i given in equation (32) is satisfied, the meridian crosses the z-axis at right angles, and simple closed "bottles" result. Where the parameters K and C_i do not satisfy equation (32), additional elements in the form of an axial compression column or tension rod located in the z-axis are necessary for equilibrium. A discussion of such shapes has been given in reference 1.

Shells containing monotropic membranes with C = 0 are, from a practical point of view, not realizable in pure form since all fibers of the C = 0 layers cross the z-axis at the same location, resulting in a "pole" singularity, and generating an impractical local buildup of material in the winding pattern at the pole. This form of pressure vessel has been approached by employing very small helix angles β_o (or small C-values). Such structures have been made in the form of the "Bermuda bottles" (C ~ 0, K ~ 2) , and as endclosures of "end-over-end" wound cylinders produced by several manufacturers of filament-wound pressure vessels.

Other possibilities in reducing the polar problem rest in the use of wide bands for the C = 0 layers.

(2) Type II (figure 22): Closed bottles of singly connected volume incorporating a secondary closure structure for the polar openings.

This type of pressure vessel needs to satisfy equation (32) for axial balance unless axial tension or compression members supporting unbalanced endclosure forces are added to the design. As seen from figure 10, all "bottles" fall in the realm of monotropic membranes in the form of corrugated tubes. These corrugated tubes can be modified to include a cylindrical portion of R = 1 between two converging portions by application of a circumferential winding pattern (C = 1) . Such "bottles" represent the ideal design for the familiar type of filament-wound cylindrical pressure vessels and rocket motor cases with "ovaloid endclosures" (reference 2).

A section of a "corrugated tube" will have two polar openings with a minimum radius of $R_{min} \gtrless C_{i_{min}}$. If a polar opening $R > C_{i_{min}}$ is required (for instance, for nozzle attachments, etc.), then a circumferential retaining hoop (C = 1) must be inserted into the winding pattern to obtain balance of an isotensoid structure requiring a special winding arrangement. In either case, a secondary closure structure, normally consisting of a flanged ring or disk insert, must be provided.

A discussion of the detail design problems for the flange attachments is beyond the scope of this report. Suffice it to note that the proper flange shapes may be derived from the basic equations for isotensoid shells by introducing the contact pressure between flange and filamentary shell into the equations.

As in the case for Type I, excessive buildup of filaments at the polar opening (i. e. , at the "turn around" point of the

winding pattern) may result. This problem can be reduced by use of a tension hoop, as discussed above, which prevents the filaments from piling up at the turn around. Other solutions that have found practical application consist of using filaments of finite width (ribbon-winding) or by small variations of the filament helix angle around a mean value (wobble-winding), which tends to spread the buildup over a finite domain of the interface area.

Containers with Doubly Connected Volume

(1) Type III (figure 23): Closed toroids (doubly connected volumes) generated from progressive loops.

Progressive loops, as shown in figure 9(a), may be used to generate close toroidal pressure vessels in two ways:

(a) A compression-resistant hub structure may be used to provide internal closure of a loop extending between two minimum perimeters R_{min} of the meridional curve. The filaments, in this case, may either be continuous around the torus meridian, or they may return around retaining hoops located at the hub rims in the fashion of an automobile tire, similar to the one shown for Type II in figure 22.

(b) A compression-resistant hoop may be introduced in the outward cusp of a single loop, providing the necessary circumferential balance forces.

In either case, compression-resistant structural components are required to close the pressure vessel. As a result, the elastic deformation of the shell due to pressurization cannot yield a geometrically similar shape which insures uniform strain in each filament. Mismatched deformations in the various components of the shell will normally take place, and deviations from ideal isotensoid conditions will be encountered in most cases.

(2) Type IV (figure 24): Closed toroids from closed loops.

Closed loops, as shown in figure 9(b), form an ideal basis

for the design of isotensoid toroidal pressure vessels, unless large access holes or valve openings are required by the particular design application.

(3) Type V (figure 25): Closed toroids generated from regressive loops.

Regressive loops, as shown in figure 9(c), may be used to form closed toroidal pressure vessels in a similar fashion, as discussed for Type III:

(a) Tension-resistant outer equatorial bands of finite width $(C = 1)$ may be used to provide external closure of a loop extending between two maximum perimeters r_o of the meridional curve.

(b) A tension-resistant hoop may be introduced in the inward cusp of a single loop, providing the necessary circumferential balance forces.

(c) Of practical importance is the case where both outer bands and an inner hoop are used for a complete torus structure. The free choice of width and/or spacing in the outer bands allows greater freedom in obtaining particular design characteristics. Further, the use of several bands allows construction of stable toroidal pressure vessel configurations with only meridional $(C = 0)$ and perimetral $(C = 1)$ windings.

As opposed to the Type III, Type V employs tension-resistant material only, thus, the conditions of uniform extension throughout the structure may be satisfied by proper dimensioning of the bands and hoops.

A review of the various isotensoid pressure vessels forming shells of revolution indicates that in practice only the toroidal Types IV and V can be made as completely closed containers and requiring only tension-resistant filamentary material.

These types promise to be of interest in two aspects:

(1) Where foldable, pneumatically stabilized structures are required, filamentary materials made from strong fibers

imbedded in an elastic matrix may be used. The absence of any rigid, compression-resistant members favors the Types IV and V for such application.

(2) Secondly, the monolithic structure of Types IV and V, and absence of additional weights due to endclosures, such as required for Type II, promises a high structural efficiency for the toroidal shapes.

Toroidal isotensoid pressure vessels which were employed for experimental verification of the theoretically derived data are discussed below.

EXPERIMENTAL STUDIES

Objectives

The experimental work reported here has been accomplished with the following objectives in mind:

1. To establish experimentally the unrestrained meridional shapes of filament-wound pressure vessels and to verify that these shapes can be predicted analytically.

2. To demonstrate the theoretically predicted load-deformation characteristics of toroidal isotensoid pressure vessels.

3. To explore failure mechanisms for this type of structure.

Experimental Method

General Approach

The objectives listed above have been satisfied by fabricating a succession of filament-wound toroids, and by measuring these under pressure. To allow the shells to assume their natural, unrestrained shapes, they have been wound on flexible, inflatable mandrels with a fine, smooth fiber. Where a bonding matrix was used, it has been applied after winding in the form of liquid elastomer.

The deformation-vs-load characteristics have been observed by subjecting the toroids to a sequence of internal pressure levels. Three distinct types of deformation have been observed:

(1)   Linear strains in the fiber systems.

(2)   Cross-sectional shape changes.

(3)   Gross changes in the toroid shape.

Material Selection and Design of Test Articles

For the structural filament, a polyester fiber in the form of an 1100 denier, untwisted, 250-end roving was chosen. This fiber has a measured breaking strength of about 15 pounds, an ultimate elongation of about 10 percent, and a cross-sectional area equivalent to about 0.013 inch solid round.

The matrix material used is a polyurethane elastomer.

The reasons for the selection of these materials are as follows:

(1)   The high elongation under load allows accurate strain measurements to be made by simple, direct means.

(2)   The excellent bending compliance of the composite material allows the pressurized shell to assume its "natural" shape, unaffected by bending stress systems resulting from incorrect initial shape.

(3)   The combination of high strength-to-weight ratio and exceptional bending compliance of the composite material used is attractive for use in efficient expandable structures.

The major portion of the test effort has been devoted to studies of the meridionally-wound toroid of Type V. The size of these toroids was taken to be that of standard automotive inner tubes since this provides a ready source of inflatable winding mandrels.

A typical cross-section for a meridionally-wound toroid is shown in figure 26.

The structure consists of three separate fiber systems:

(1) A meridional winding.

(2) An inner equatorial band.

(3) An outer equatorial band.

Other layers of material shown in figure 26 are non-structural and result from the fabrication process.

Design data are given in Table I for two typical meridionally-wound toroids.

Fabrication of Test Articles

The fabrication of the various toroids has been accomplished with the aid of the toroid winder shown in figure 27. A typical procedure is as follows:

(1) An automotive inner tube has been used as a winding mandrel. The tube is prepared by replacing the standard valve with a flush-mounted basketball valve installed on the outer equator. The tube is then brought to the correct meridional perimeter by wrapping with polyester film tape of controlled length per turn.

(2) The inner equatorial band, prepared on a separate mandrel, is then taped in place on the inner equator of the tube.

(3) The tube is covered with a layer of light-weight nylon cloth to insure against premature failure due to meridional splits.

(4) The meridional winding of structural fiber is then applied by the toroid winder. The fiber is either pre-impregnated or the winding is soaked with dilute elastomer and cured to form the rubber-fiber composite material.

(5) The outer band, prepared separately, is then installed. The valve hole in the outer equator is kept clear by making slits in the windings parallel to the fibers.

Test Instrumentation

The instrumentation used in the strain-vs-pressure tests has been designed to measure the toroid deformation in three different modes:

(1)   Linear elongation of typical fibers in each fiber system.

(2)   Volumetric expansion.

(3)   Change of meridional shape.
The particulars of the various measurements are given in Table II.

Figure 28 shows a diagram of the toroid cross-section, indicating the various measurements which were made.   Figure 29 shows the test set-up for toroid measurements with the extensometers used to measure changes in meridional and equatorial lengths and the polar-coordinate ring used to determine the meridional shape.

The toroid is pressurized by a motor-driven gear pump, which transfers water from a weighable reservoir to the toroid.   The volume change is determined from the reservoir weight.   The initial volume is determined by weighing the toroid before and after filling with water.

Test Procedure

The polyester fiber used in this test program shows peculiar elastic effects involving hysteresis and strain rate transients.   These were determined by a series of load-elongation tests made with single fibers, bands, and cylinders.   Typical results from these tests are shown in figures 30 and 31.   The effects of this behavior have made it necessary to standardize on a fixed schedule for tension vs time in all tests used for comparison of toroid tests to nominal materials properties in order to obtain a reproducible tension-vs-strain diagram.

The time intervals in the tension-vs-time schedule for the toroid tests were determined by the requirements of the test itself.   It was found that five minutes were required to complete the readings at each pressure level, and that a settling time of ten minutes was required for the strain to settle to an essentially constant value over the reading period.

In order to determine the pressure which corresponds to a given tension level, considering the large deformations that occur, the procedure described in Appendix C has been used, along with a prediction of the strain at each level of tension, based on preliminary load-strain tests of the fiber composite material.

Results

Instability Characteristics

Instability phenomena have been observed in toroidal pressure vessels and reported, for instance, in reference 14. Such instabilities will be expected particularly in those cases which are of structurally underdeterminate nature, i. e., in shells containing two or less fiber directions in certain domains of the structure. The instability mechanisms are similar to those observed in magnetic bottles designed to confine plasma at high pressure, where the magnetic lines of force take the place of the filamentary texture (See, for instance, reference 15). Other mechanisms of this type are those found in soap bubbles (reference 16) or may be of the nature of the "hydrostatic instabilities" observed in straight cylindrical tubes made from isotropic material (reference 17).

Early tests of meridionally-wound toroids showed that similar instabilities are apt to exist in these structures. Large-deformation failure modes arise from the tendency of the toroid to increase volume at the expense of locally high shear and normal strains in the matrix material which bonds the meridional fibers together.

Two different modes of this type of buckling have been observed:

(1) "Rolling" Modes

    If the toroid consists of a meridional winding which is restrained circumferentially by an outer band only, (Type V(a)), the toroid will exhibit a tendency for the meridional loops to roll over and out of the equatorial band. This type of deformation is shown in figure 32.

(2) "Baseball Seam" Modes

    If the toroid consists of a meridional winding restrained by

an inner band only, (Type V(b)), the toroid will buckle by curling into a "baseball-seam" curve. Several types of this mode are shown in figures 33 through 36, some exhibiting striking geometrical symmetry and beauty.

Strain Distribution

The results of the strain measurements made during the test of Toroid #4 are shown in figure 37. The solid curve in the figure is a plot made from tests of the material. The plotted points represent measured values of strain vs pressure (reduced to fiber tension by the method outlined in Appendix C).

Note that the volumetric strain (as defined in Appendix C) is consistently greater than the strain in the meridian or that in the outer equator measured along its average circumference. This observation points to an inherent inadequacy in this particular design; without anomalous volume growth, the rolling could be attributable, for example, to a combination of small manufacturing errors and high sensitivity of the design to such errors.

The strain measurements obtained during test of Toroid #5 are shown in figure 38 along with a curve of the nominal properties of the fiber obtained from tests under equal load sequence.

The slight tendency to roll is exhibited by the three strain measurements made on the outer equatorial band. This roll distortion caused the inner band to be shifted about 0.2 inch from the predicted plane of symmetry prior to failure. However, the volumetric strain was not significantly different from the other strain measurements.

Cross-Sectional Shapes

A comparison of the cross-sections of Toroid #5 at two pressure levels with the theoretical curves is shown in figure 39. The heavy curve shown is the theoretical isotensoid meridional torus section, which is a composite of two isotensoid curves connected at the outside by the outer band and at the inside by a rounded corner representing the inner band contour. The light curve is a geometrically similar enlargement of the heavy curve, using the toroidal-coordinate origin as the invariant point. The enlargement factor is 1.07 (i.e., 7 percent strain) corresponding to a fiber tension of 9 pounds.

The points plotted along these meridional curves represent measurements of the cross-section made with the polar coordinate ring shown in figure 29. The points marked with circles are from a measurement at 15 psi internal pressure or about 0.5 pounds per fiber, while the solid points represent the cross-section at 240 psi internal pressure or 9 pounds per fiber.

In each case, the measured points have been located radially with respect to a point obtained from a measurement of the outer equator length. Hence, the corresponding sets of experimental and theoretical cross-sectional data have been placed on the diagram independently from each other; these data are related through the curve of nominal fiber properties (i.e., 7 percent strain at 9 pounds tension) but otherwise bear no direct relation.

Examination of the data obtained at low pressure reveals that the meridian is initially more nearly circular than theoretically predicted. This is attributable to the fabrication process: the matrix material was applied and allowed to cure at low internal pressure of the toroid. The initial shape, therefore, is influenced by the inner-tube which tends to approach a circular section.

At the higher pressure level, the load carried by the fiber is large compared with the load carried transversely by the matrix and rubber tube, and the meridional shape is determined primarily by the fiber. In this case the comparison between the theoretically predicted and the measured meridional shapes shows excellent agreement. In the full-scale layout, the experimental points all fall within .03 inch of the theoretical curve.

Additional cross-section measurements have been made with a toroid of Type V(a) with inner band only (Toroid #3), shown completed in figure 40, and with a helix-wound toroid of Type IV (Toroid #6) shown in the process of fabrication in figure 27.

Fair agreement between measured and theoretical ("isotensoid") meridional cross-sections for both toroids are shown in figures 41 and 42.

Astro Research Corporation
    Santa Barbara, California, July 20, 1961

APPENDIX A

MONOTROPIC SHELLS SUBJECT TO
CENTRIFUGAL LOADING AND PRESSURE

Consider a monotropic membrane in the form of a shell of revolution similar to the one shown in figure 5.

In addition to the normal load/unit length of filament due to a uniform internal pressure, also consider a radial load vector $\overline{F}'_\omega$ caused by a rotation of the shell around the z-axis with an angular velocity ω .

$$\overline{F}'_\omega = m' r \omega^2 \begin{pmatrix} \cos\varphi \\ \sin\varphi \\ 0 \end{pmatrix} \tag{1-A}$$

where m' is the mass associated with a unit length of the filament.

The tangential component of this load vector is obtained by scalar multiplication with the unit tangent vector $\overline{e}_t$:

$$F'_t = \left(\overline{F}'_\omega \cdot \overline{e}_t \right) = m' r \omega^2 \cos\beta \sin\alpha \tag{2-A}$$

The first equilibrium equation (13) becomes

$$\frac{dT}{ds} + m' r \omega^2 \cos\beta \sin\alpha = 0$$

and, since $dr = - ds \cos\beta \sin\alpha$:

$$dT = m' r \omega^2 dr$$

which integrates to

$$T - T_o = m \omega^2 \frac{1}{2} \left(r_o^2 - r^2 \right)$$

or

$$\frac{T}{T_o} = 1 + \frac{\Omega}{2} \left(1 - R^2 \right) \tag{3-A}$$

where T_o is the fiber force at r_o and $\Omega = \dfrac{m' \omega^2 r_o^2}{T_o}$ is the non-dimensionalized centrifugal load parameter. Thus, the fiber force is non-uniform and an "isotensoid" design would require a tapering cross-section of filaments designed to keep the filament stress and strain uniform.

The equilibrium conditions for the shell of revolution in axial direction and in torque remain unaffected by the centrifugal force field. Thus, equation (25a) becomes, for a single monotropic membrane

$$T \sin\beta \ R \ = \ T_o \ C \qquad\qquad (4\text{-}A)$$

Since, in general, T/T_o will differ from unity, the fiber paths are obviously no longer geodesics. This may be verified by comparing equation (4-A) with Clairaut's Theorem given in the form of equation (25a).

The axial equilibrium equation (30) becomes for a single monotropic membrane:

$$n \ T_o \ \cos\beta_o \ - \ r_o^2 \ \pi \ p \ = \ n \ T \ \cos\alpha \ \cos\beta \ - \ R^2 r_o^2 \ \pi \ p$$

$$\text{or} \quad \sqrt{1 - C^2} \ - \ \frac{K}{2} \left(1 - R^2 \right) \ = \ \cos\alpha \ \sqrt{\left(\frac{T}{T_o} \right)^2 - \frac{C^2}{R^2}} \qquad (5\text{-}A)$$

where K is defined by

$$K \ = \ \frac{2\pi \ r_o^2 \ p}{n \ T_o}$$

Solving equation (5-A) for $\cos\alpha$ and substituting equation (3-A) for T/T_o yields the intrinsic equation for the meridional shape of a monotropic membrane subject to both a uniform internal pressure

and a distributed centrifugal load associated with a rotation around the z-axis and a uniform mass distribution per unit length of the filaments:

$$\cos\alpha = \frac{\sqrt{1 - C^2} - \frac{K}{2}\left(1 - R^2\right)}{\sqrt{\left[1 + \frac{\Omega}{2}\left(1 - R^2\right)\right]^2 - \frac{C^2}{R^2}}} \tag{6-A}$$

Thus, the equilibrium shape is defined by three characteristic parameters:

(1) The parameter defining the fiber geometry: C .

(2) The parameter defining the pressure loading: K .

(3) The parameter defining the centrifugal loading: Ω .

38

APPENDIX B

MERIDIONALLY WOUND ISOTENSOID PRESSURE VESSELS

For the particular case of $C \equiv 0$ (i.e., meridional fiber direction only) and for $p = p_o$ = Constant , equations (29) and (30) reduce to

$$\frac{r_o}{\rho_M} = K R \qquad (1\text{-}B)$$

$$\cos\alpha = 1 - \frac{K}{2}(1 - R^2) \qquad (2\text{-}B)$$

It can be shown (reference 18) that the shape of a buckled slender column with large deformations, subject to eccentrical loading, as shown in figure 6, satisfies an equation of the form (1-B) as follows:

Let   EI = bending stiffness of column

     - P = compressive load

Then the equilibrium condition for the buckled column becomes

$$Pr = \frac{EI}{\rho}$$

or

$$\frac{1}{\rho} = \frac{P}{EI} r \qquad (3\text{-}B)$$

which can be transformed into equation (1-B) by setting

$$K = \frac{P r_o^2}{EI}$$

Analytical solutions to this classical problem ("The Elastica") lead to tabulated elliptical integrals of the first and second kind (reference 13), and have been worked out in detail by several authors

(See, for instance, references 19 and 20). The derivations will not be reproduced here, but only the principal results will be summarized.

The lengths s of the column (or meridional lengths of the isotensoid pressure vessel) is related to the parameter $K = \dfrac{P\,r_o^2}{EI}$ by

$$\frac{s}{r_o} = \frac{2}{\sqrt{K}}\; \mathfrak{F}\left(\hbar,\; \frac{\pi}{2}\right) \tag{4-B}$$

where

$\mathfrak{F}$: Elliptical integral of the first kind

$\hbar = \dfrac{\sqrt{K}}{2}$: Characteristic argument of elliptical integral.

The maximum deflection r_o of the column (or perimetral radius r_o of the isotensoid pressure vessel) is:

$$r_o = \frac{\hbar s}{\mathfrak{F}\left(\hbar,\; \dfrac{\pi}{2}\right)} \tag{5-B}$$

The distance h between ends of the buckled column (or between the poles of the isotensoid membrane) is:

$$\frac{h}{r_o} = \frac{1}{\hbar}\left[2\mathcal{E}\left(\hbar,\; \frac{\pi}{2}\right) - \mathfrak{F}\left(\hbar,\; \frac{\pi}{2}\right)\right] \tag{6-B}$$

where

$\mathcal{E}$: Elliptical integral of the second kind.

The "column analogy" for the meridional isotensoid uniform pressure vessel has proven useful in gaining insight into the types of solutions that can be expected. A workable analog device suitable for general study has been constructed from a thin piano wire, loaded by axial forces over adjustable bars, as shown in figure 7.

Several solutions for the case $C = 0$ are shown in figure 11. Their general character shows a peculiarity, which has been discussed in reference 1.

The cusp case $(K = 2)$ represents a closed ovaloid (Bermuda bottle). Alternating loops crossing the z-axis between each maximum occur between $K = 2$ and $K = 4$. These loops are progressive for $2 < K < 3.32$ and regressive for $3.32 < K < 4$. The transition case of $K = 3.32$ represents a figure resembling a lemniscate from which a degenerated closed toroid of vanishing inner perimeter can be formed by rotation around the z-axis.

The case $K = 4$ represents an aperiodic loop with both branches asymptotic to the z-axis.

For $K > 4$, regular, regressive periodic loops such as shown in figure 9(c) occur.

APPENDIX C

SUMMARY OF DATA REDUCTION RELATIONS

Calculation of Fiber Tension from Pressure

In order to reduce the pressure-vs-elongation data to terms of tension vs strain for the meridional toroids, the effect of large deformations must be taken into account. This is accomplished as follows:

The fiber tension in the meridional winding is given by:

$$T = \frac{2\pi p r_o^2}{n_m K}$$

where

p = pressure

r_o = radius of outer equator

K = pressure load parameter

n_m = number of fibers in the meridional windings

Let $\left(r_o\right)_o$ denote the initial value of the outer equatorial radius, at zero pressure. Let ϵ denote the fiber strain.

Then,

$$r_o = \left(r_o\right)_o (1 + \epsilon)$$

and,

$$T = \frac{2p}{n_m K} \left(r_o\right)_o^2 (1 + \epsilon)^2$$

Calculation of Volumetric Strain

The volumetric strain is defined as the non-dimensional linear scale increase which would correspond to a given increase in volume if that volume increase resulted from a geometrically similar expansion of the pressure vessel. Thus, if ϵ_V is the "volumetric strain" corresponding to a volume increase ΔV from an initial volume V_o, then,

$$V_o + \Delta V = V_o (+ \epsilon_V)^3$$

This yields the "volumetric strain," as,

$$\epsilon_V = \sqrt[3]{1 + \frac{\Delta V}{V_o}} - 1$$

REFERENCES

1. Hoffman, G. A. : The Effect of Filamentary Materials on Pressure Vessel Design. International Astronautical Congress, Stockholm, Sweden, August 1960.

2. Young, R. E. : History and Potential of Filament Winding. 13th Annual Technical and Management Conference, Reinforced Plastics Division, Society of the Plastics Industry, Chicago, Illinois, 4 February 1958.

3. Riley, M. W. , and Lieb, J. H. , et al: Filament Wound Reinforced Plastics: State of the Art. Reprint from Materials in Design Engineering, August 1960.

4. Proceedings, Filament Winding Conference. Society of Aerospace Material and Process Engineers, 28-30 March 1961.

5. Schuerch, H. U. : Preliminary Study of Application of Advanced Structural Materials to Space Vehicles and Boost Systems. General Electric - TEMPO, RM59TMP-9, 31 January 1959.

6. Hedgepeth, J. M. : Stress Concentrations in Filamentary Structures. NASA TN D-882, 1961.

7. Brenner, S. S. : Growth and Properties of Whiskers. Science, Volume 128, 12 September 1958.

8. Green, A. E. , and Adkins, T. E. : Large Elastic Deformations and Non-Linear Continuum Mechanics. Oxford University Press, 1960.

9. Struick, D. J. : Differential Geometry. Addison Wesley Press, 1950.

10. Haack, Wolfgang: Elementare Differential Geometrie. Birkhauser Verlag Basel, 1955.

11. Coxeter, H. S. M. : Introduction to Geometry. John Wiley, Inc. , 1961.

44

12. Scarborough, J. B. : Numerical Mathematical Analysis. John Hopkins Press, 1950.

13. Jahnke, E. , and Emde, F. : Tables of Function. Dover Publications, 1945.

14. Schuerch, H. U. : Space Structure Design with Composite Materials. Astro Research Corp. , ARS Preprint 1096-60, April 1960.

15. Koller, A. : Confining A Plasma by A Magnetic Field. ASTIA Doc. No. AD-254 017, April 1961.

16. Boys, C. V. : Soap Bubbles, Their Colours and the Forces Which Mold Them. Dover Publications, 1959.

17. Mills, B. D. , Jr. : The Fluid Column. American Journal of Physics, Volume 28, No. 4, April 1960.

18. Schuerch, H. U. , and Kyser, A. C. : Isotensoid Torus Design - Final Report. Astro Research Corp. , Contract NAS 1-889, 16 February 1961.

19. McLachlen, R. : Ordinary, Non-Linear Differential Equations. Oxford University Press, 1956.

20. Southwell, R. V. : Theory of Elasticity. Oxford University Press, 1946.

TABLE I

TYPICAL DESIGN DATA FOR TOROIDS

(Dimensions in Inches)

	TOROID # 4	TOROID # 5
GENERAL		
Outside Diameter (in.)	27.2	28.9
Pressure load parameter K	5.7	5.0
Volume (cu. in.)	2130	3180
Surface area (sq. in.)	1340	1640
Initial p/T, psi per lb.	26.9	30.0
Area of meridional loop (sq. in.)	31.8	46.8
Minimum radius for concentrated inner band (in.)	7.5	6.68
MERIDIONAL WINDING		
Perimeter (in.)	20.0	24.5
Number of turns	5560	7900
OUTER EQUATORIAL BAND		
Inner diameter (in.)	27.2	28.9
Number of turns	550	750
Width (in.)	1.5	1.7
INNER EQUATORIAL BAND		
Inner diameter (in.)	15.0	13.6
Number of turns	280	650
Width (in.)	0.6	1.2

TABLE II

DETAILS OF MEASUREMENTS

MEASUREMENT	INSTRUMENT	PRECISION
Meridian length	Extensometer	0. 1%
Outer band length	Extensometer	0. 1%
Inside diameter	Steel tape	0. 1%
Volume change (reservoir wt.)	Platform scale	0. 05%
Meridian shape	Polar-coord. ring with dial gage probe	0. 1% of min. rad. of curve
Elev. of inner equator Elev. of outer equator Elev. of top meridian	Height gage from horizontal surface to marks on toroid	0. 2%
Pressure	Bourdon gage	0. 3% of max.
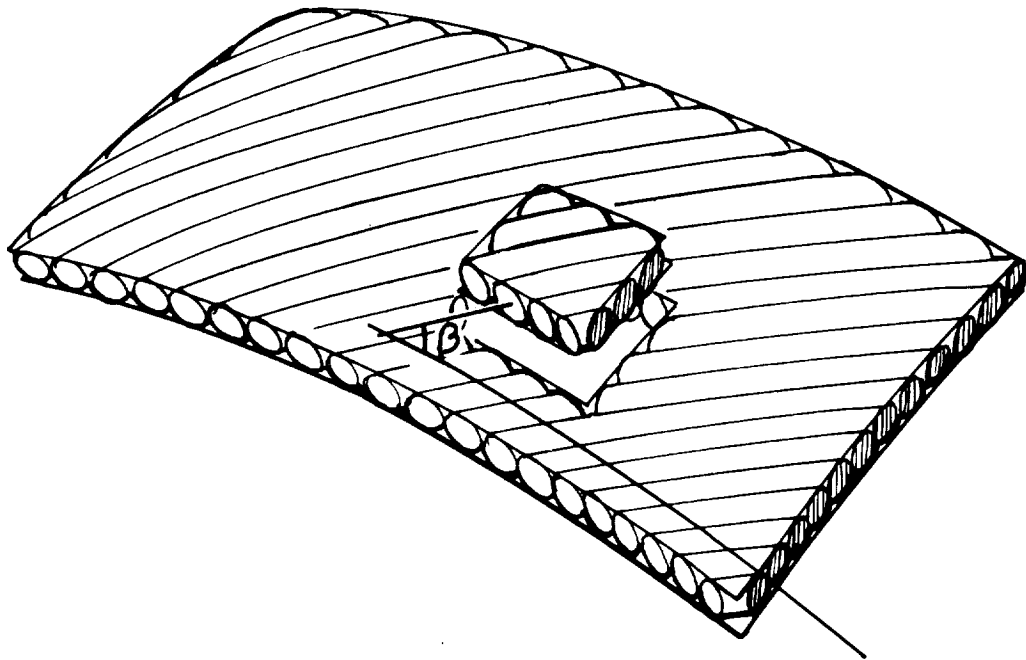
Figure 1. - Monotropic Membrane.
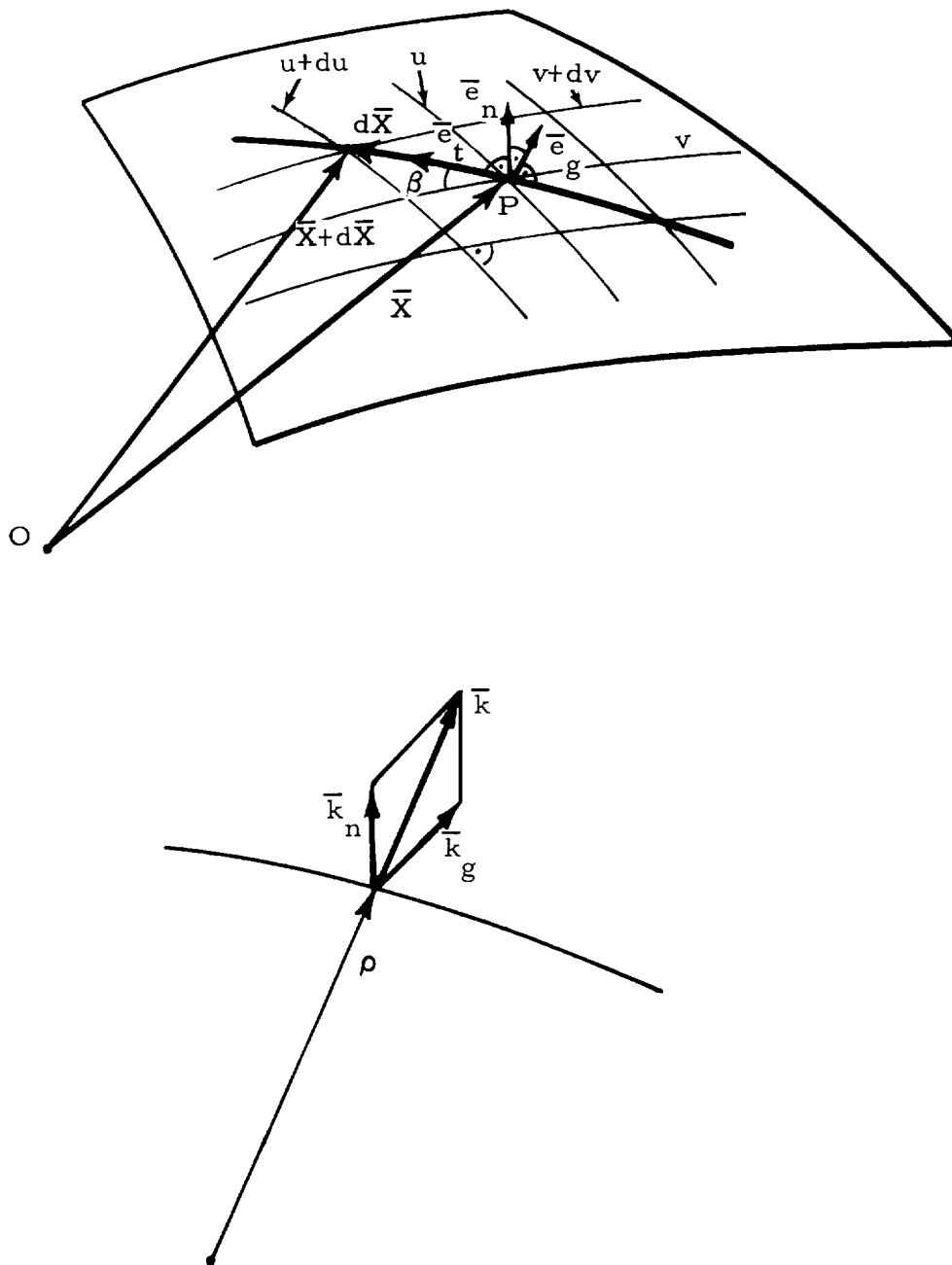
Figure 2. - Coordinate Systems and Fiber Geometry for
Generalized Surface.
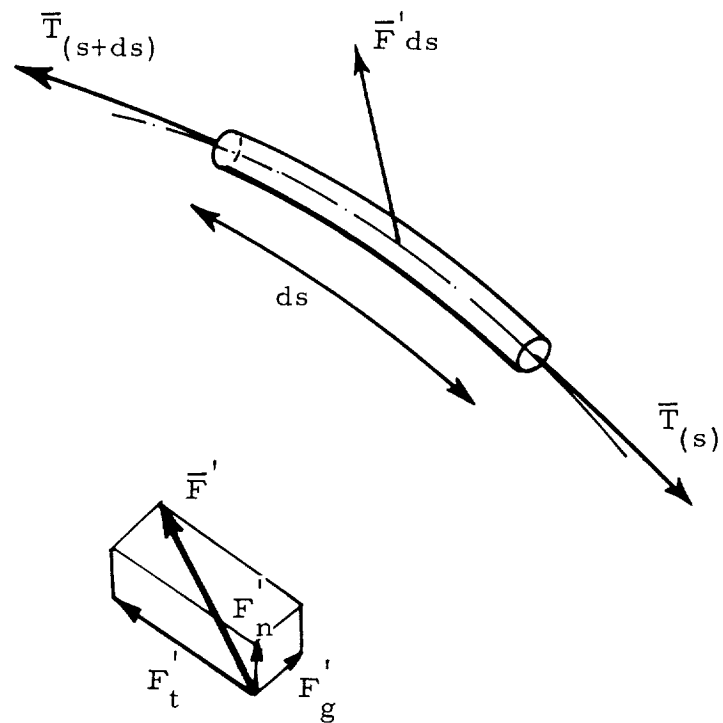
Figure 3. - Forces on Filament Element.
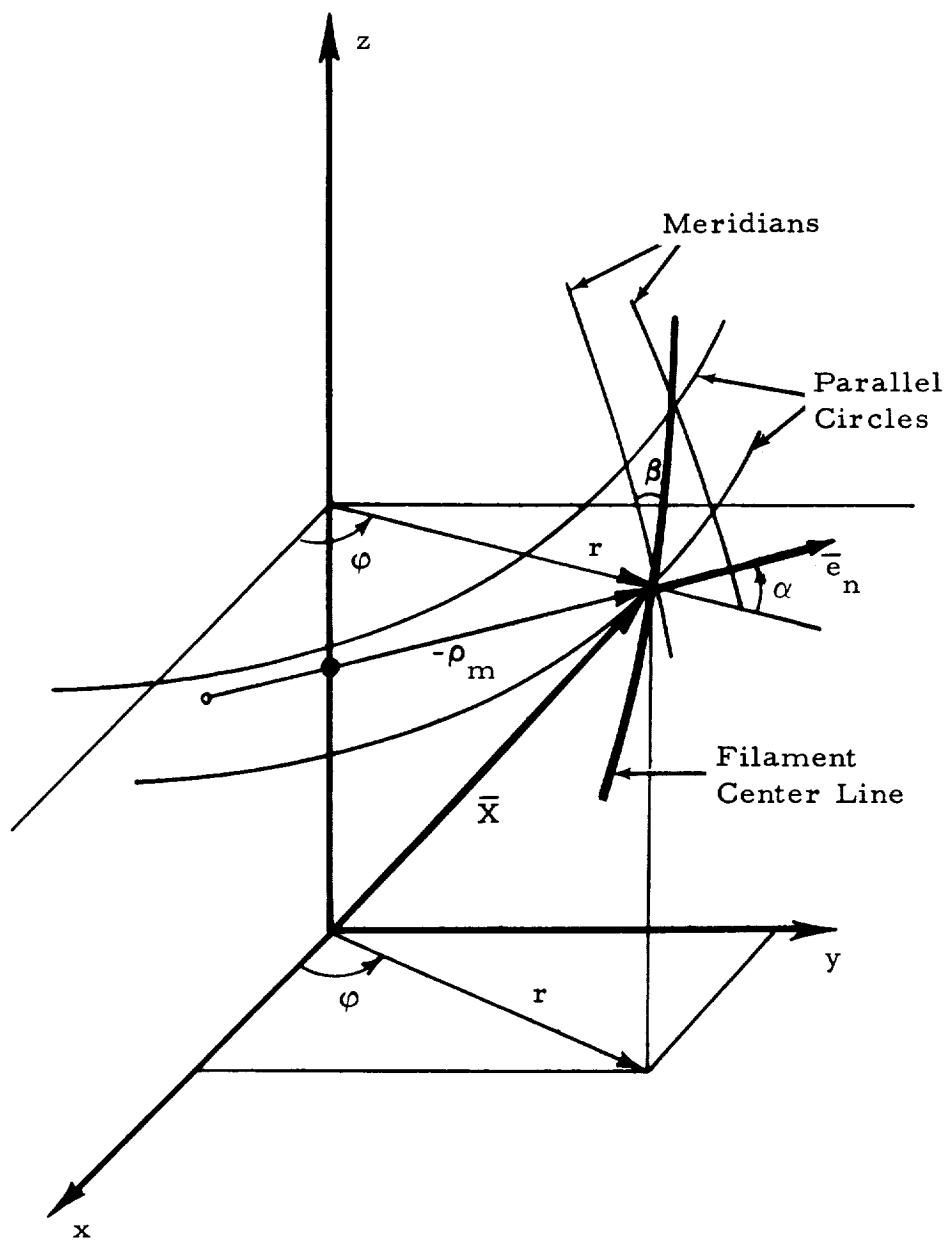
Figure 4. - Coordinate System and Fiber Geometry for
Surface of Revolution.
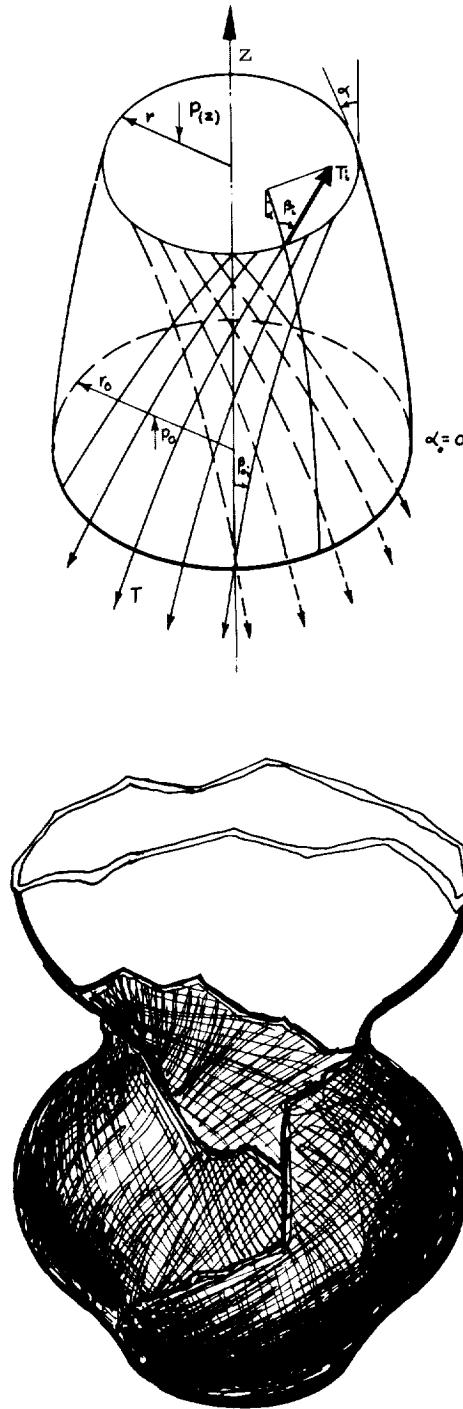
Figure 5. - Pressure Loaded Shell Made from Several
Layers of Monotropic Membranes.
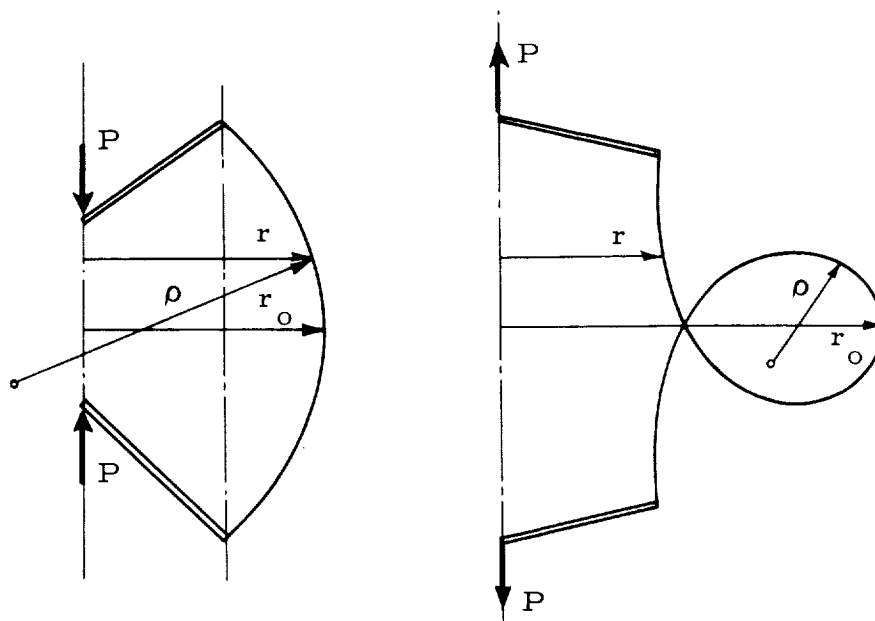
Figure 6. - Column Analogy.
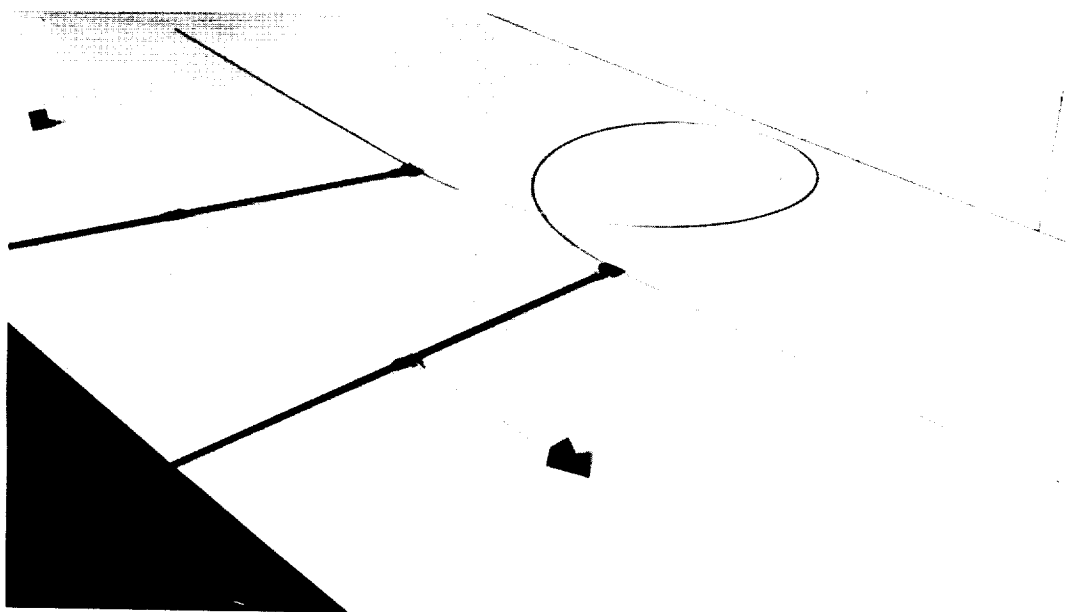
Figure 7. - Column Analog Apparatus.
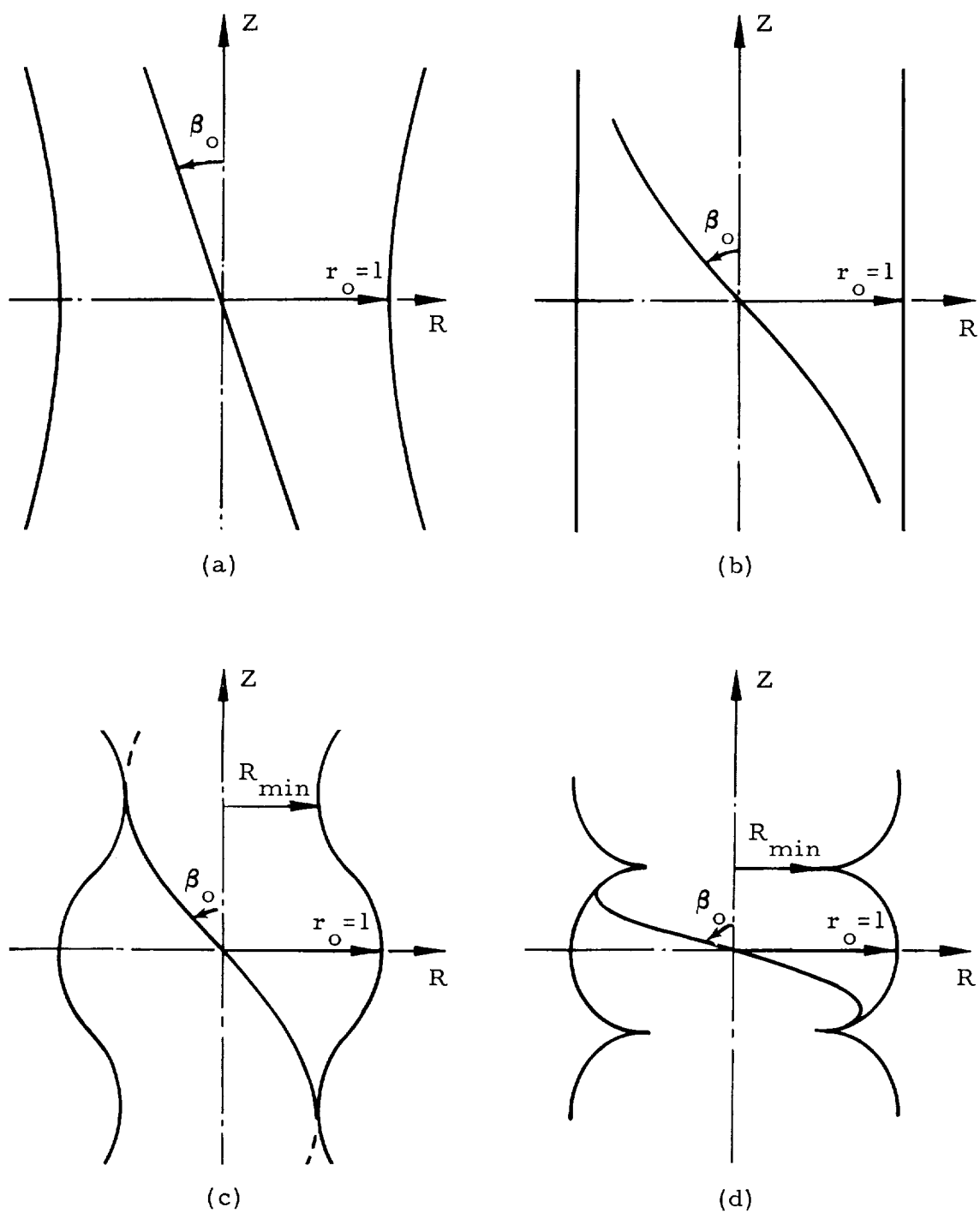
Figure 8. - Isotensoid Meridional Shapes.
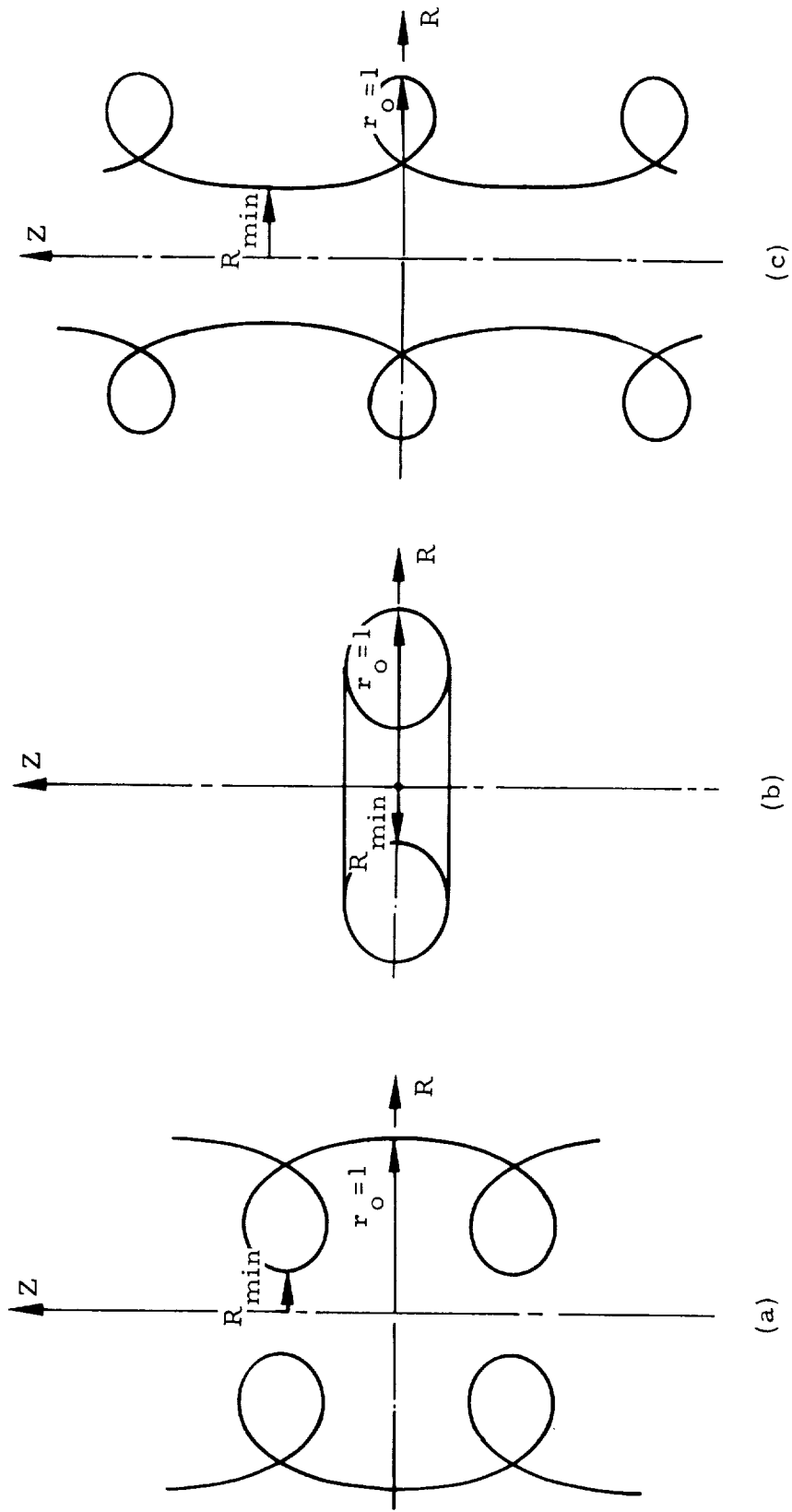
Figure 9. – Isotensoid Meridional Shapes.
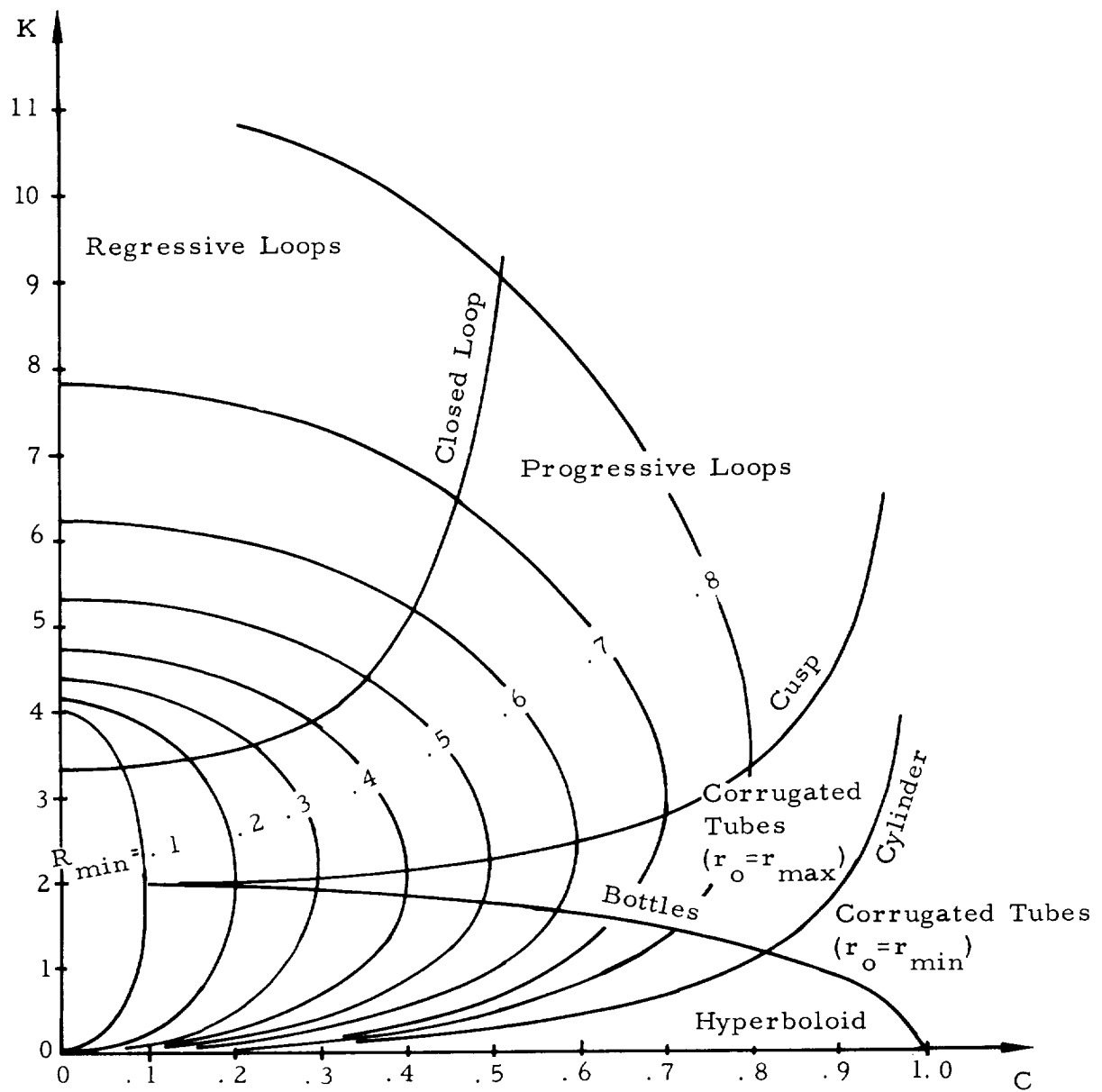
Figure 10. - Isotensoid Domains in Function of the
Parameters C and K.
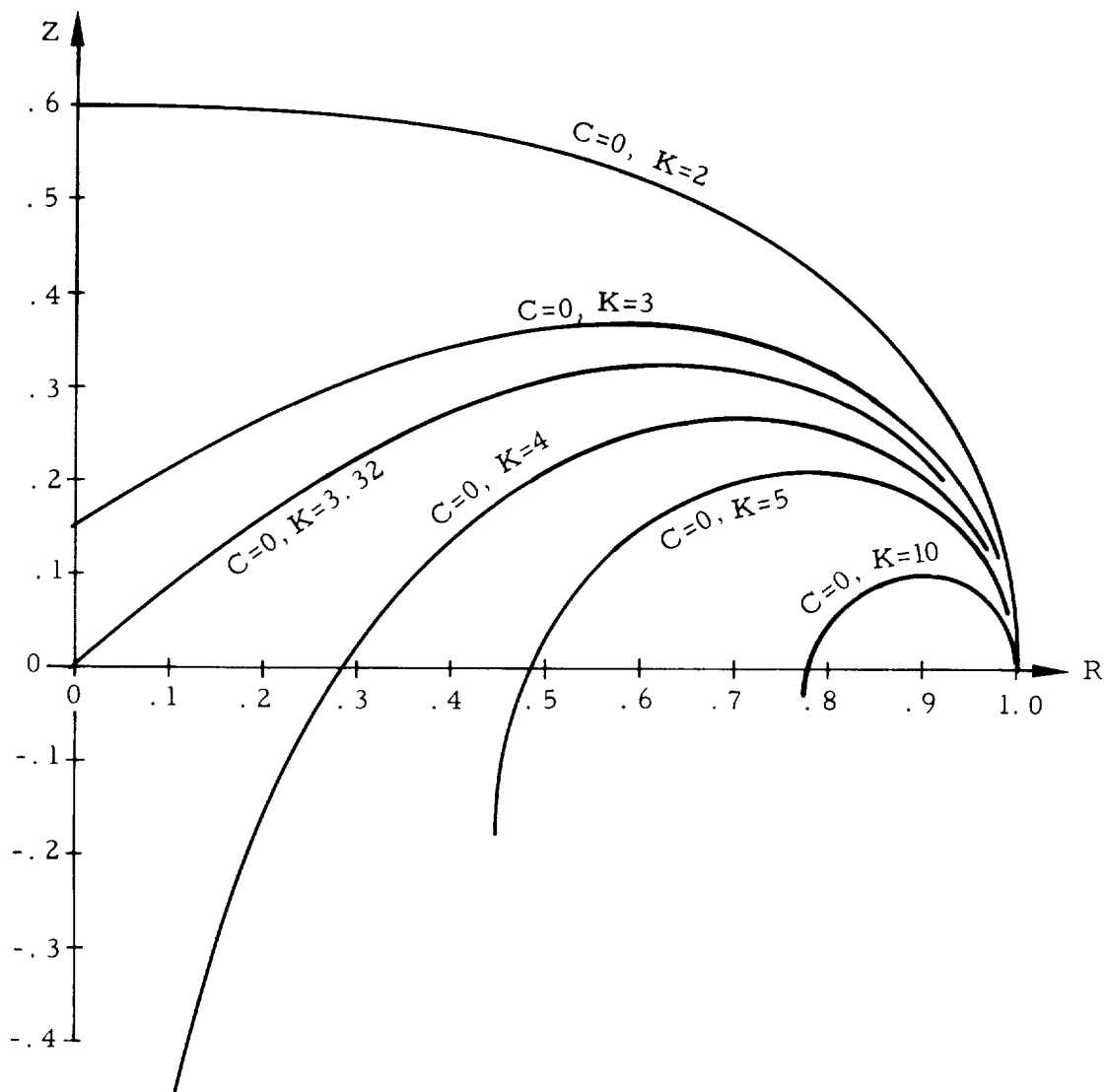
Figure 11.- Isotensoid Shapes for C = 0.
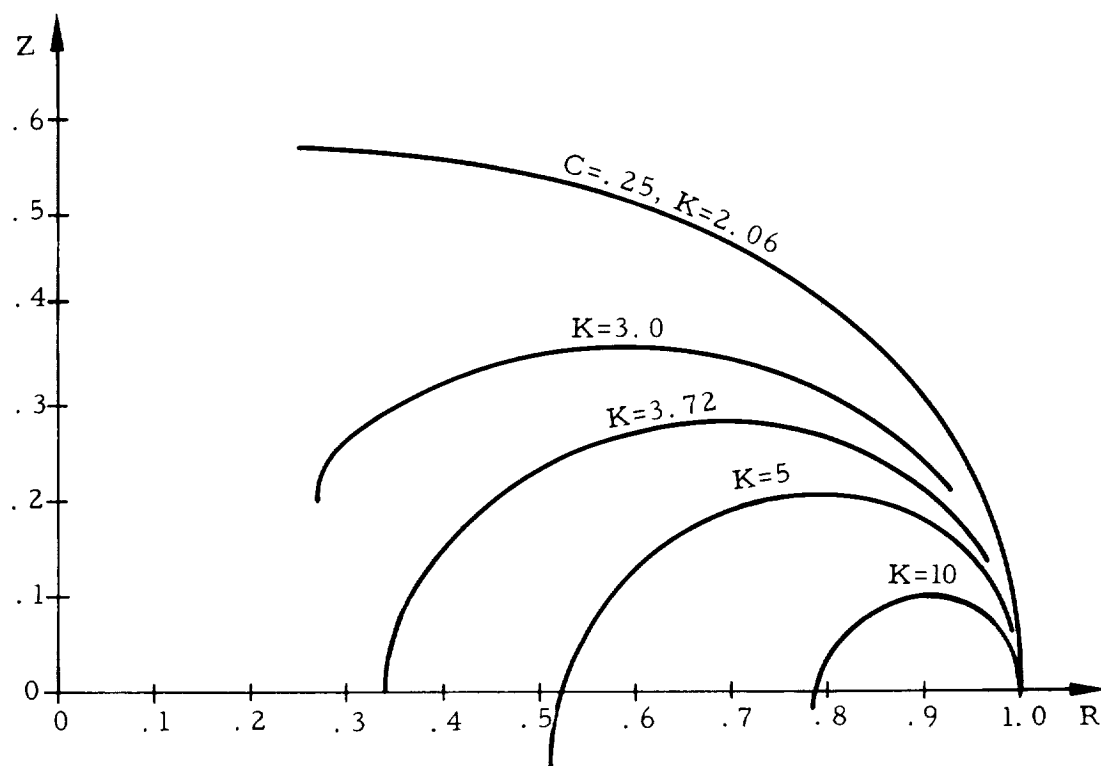
Figure 12. - Isotensoid Shapes for C = ± .25.
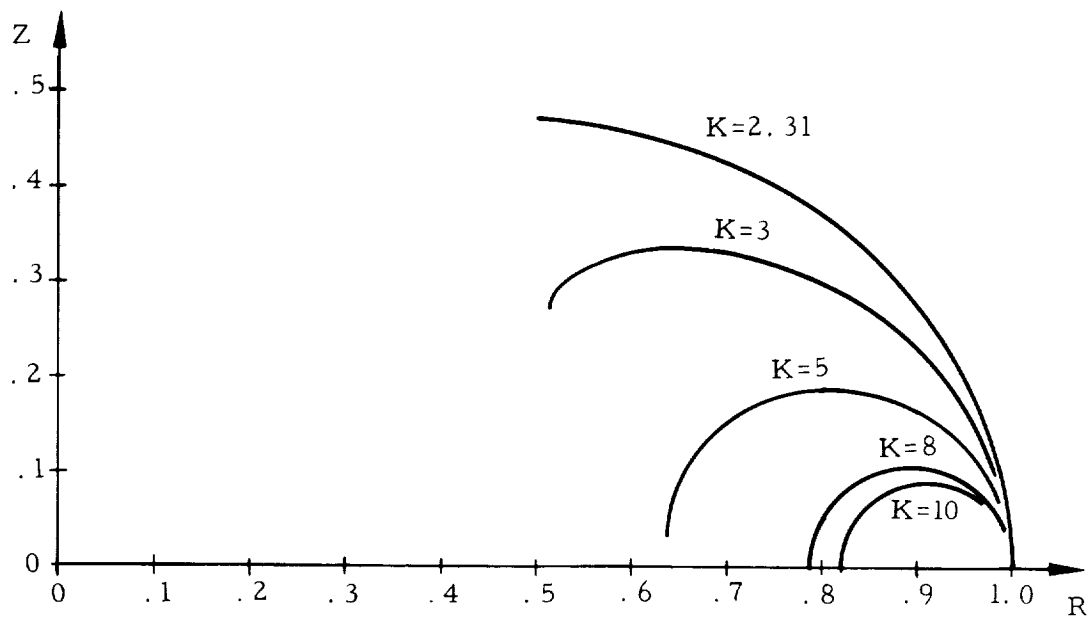
Figure 13. - Isotensoid Shapes for C = ± .50.
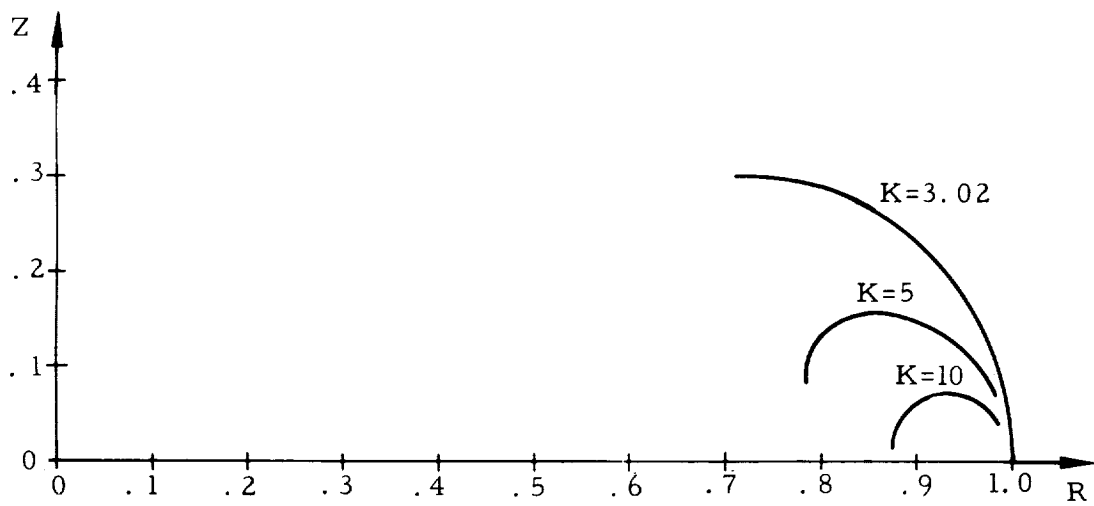
Figure 14. - Isotensoid Shapes C = ± .75.

Figure 15. - Isotensoid Shapes for Multiple Helix Angles.

$$C_1 = 0 \qquad C_2 = .5 \qquad C_3 = -.5$$

$$N_1 = .5 \qquad N_2 = .25 \qquad N_3 = .25$$

Figure 16. - Isotensoid Shapes for Multiple Helix Angles.

$C_1 = O$ $C_2 = .5$ $C_3 = -.5$

$N_1 = .75$ $N_2 = .125$ $N_3 = .125$
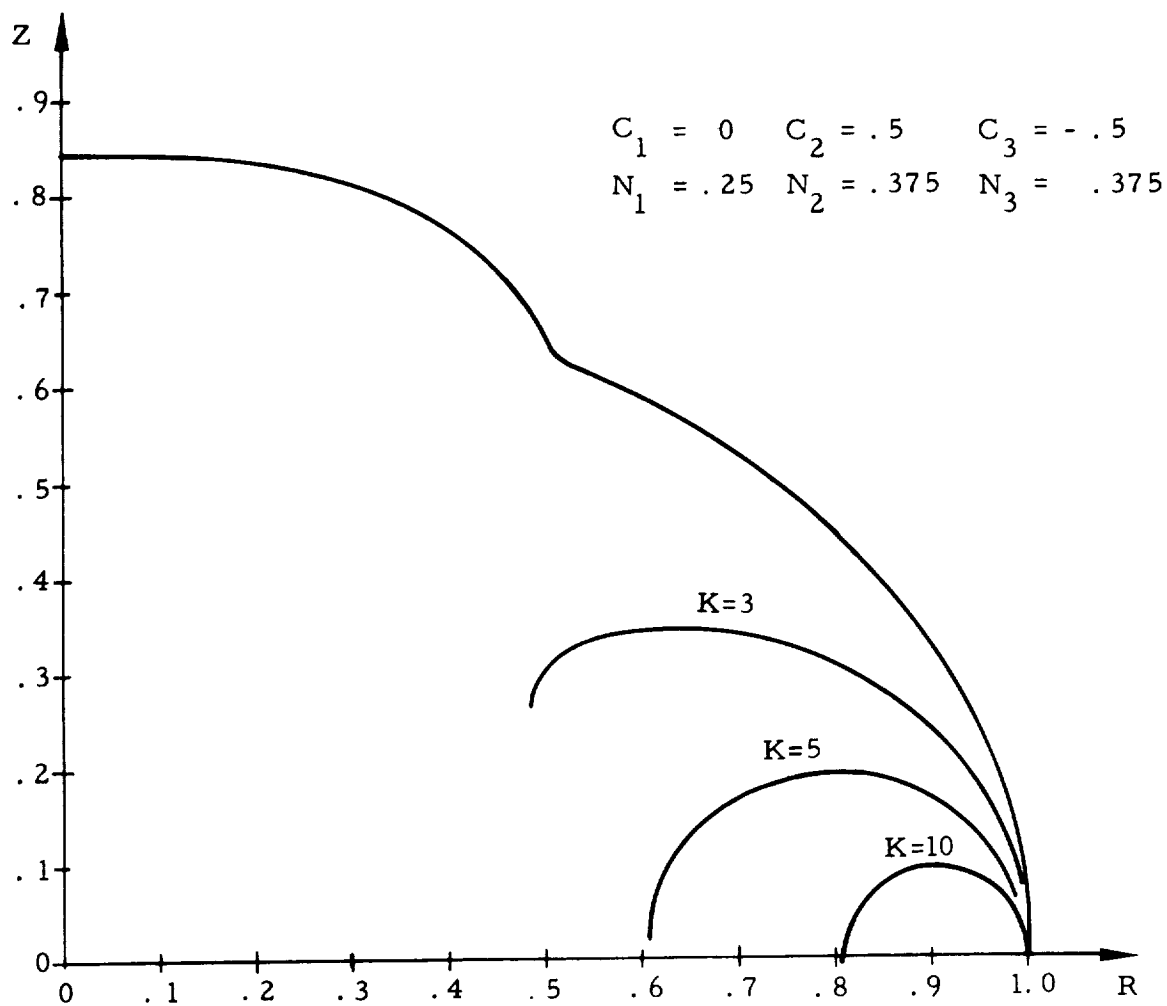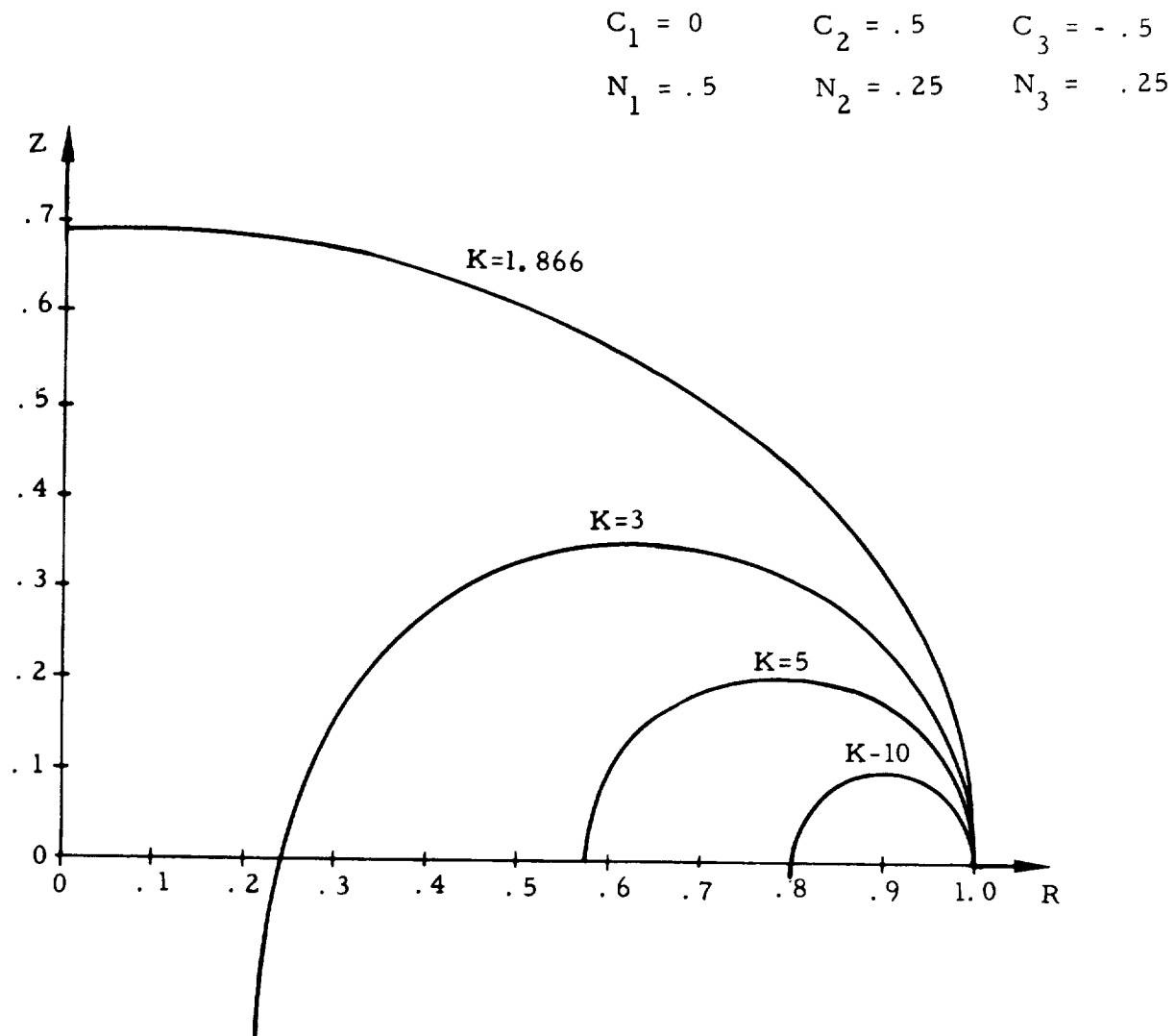
Figure 17.- Isotensoid Shapes for Multiple Helix Angles.
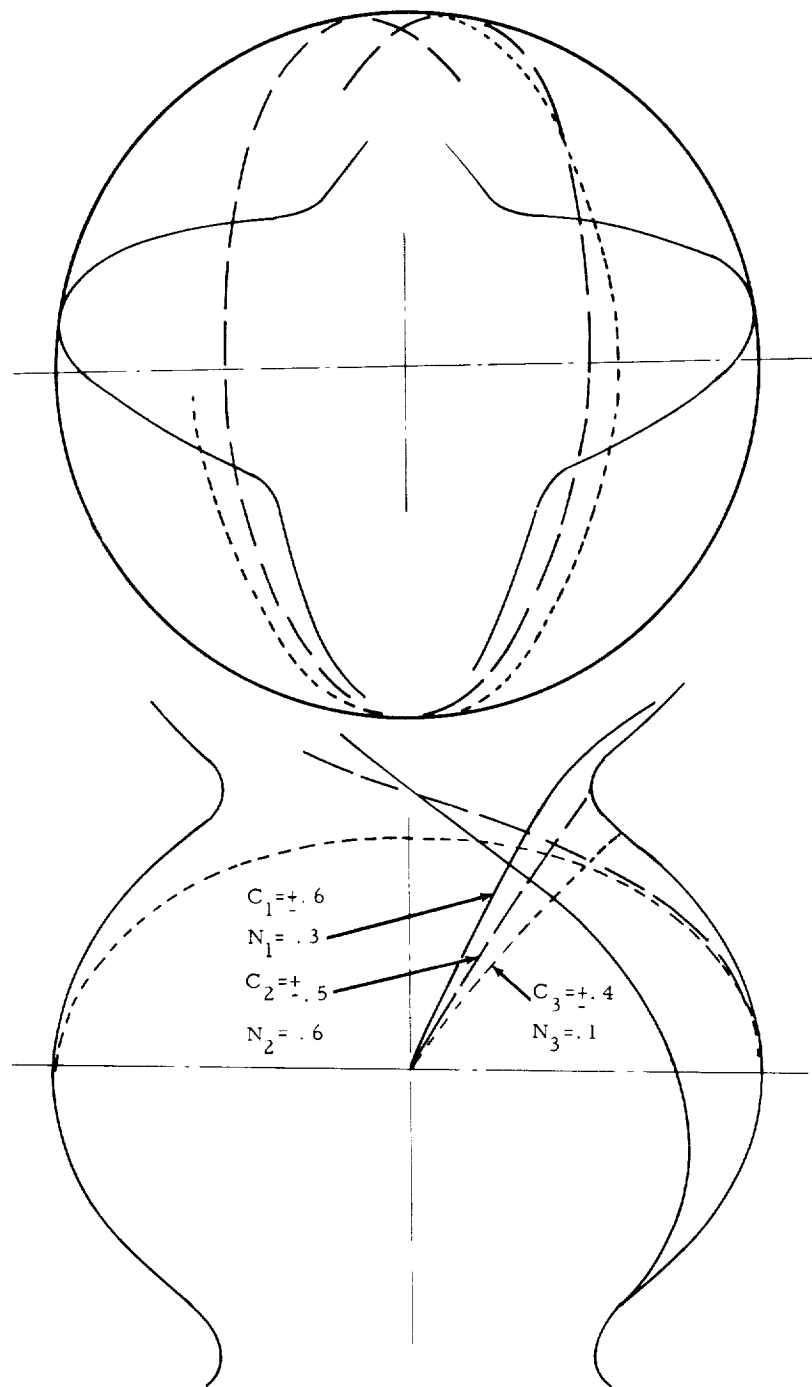
Figure 18. - Schematic of Isotensoid Shape and Fiber Geometry
for Multiple Layered Corrugated Tube k = 1.7.
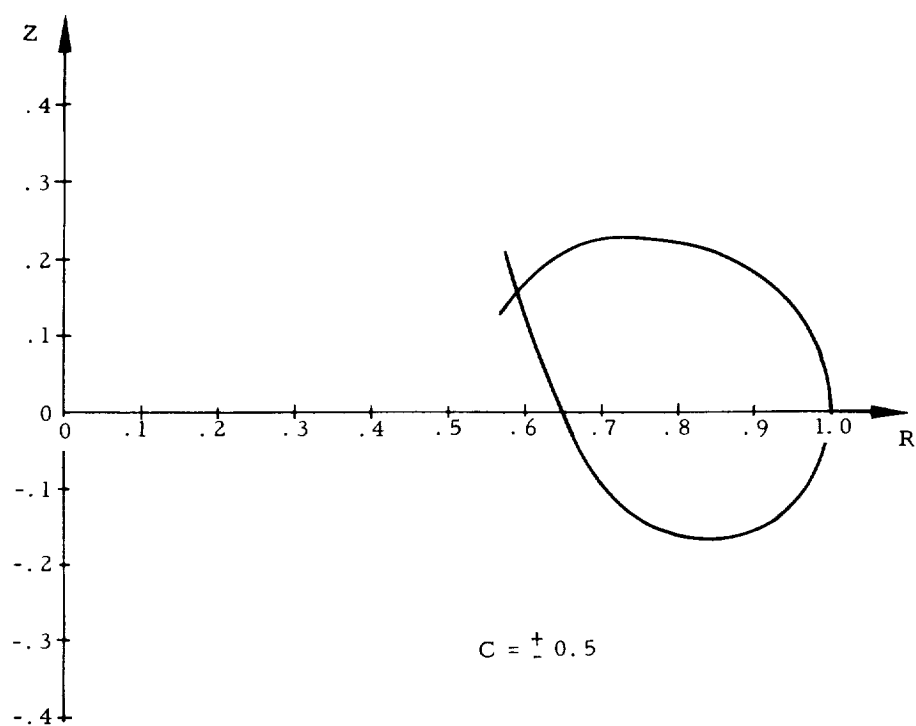
Figure 19. - Isotensoid Shape for Linear Pressure Gradient.
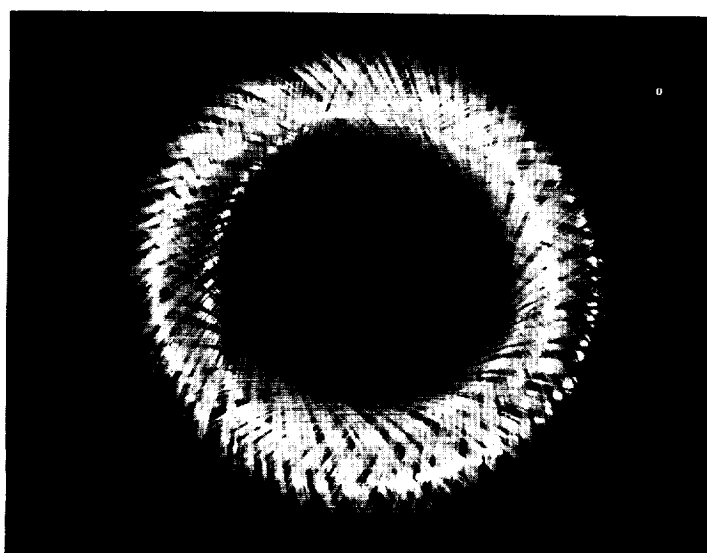
Figure 20. - Isotensoid Shape and Filament Geometry
for Closed Torus C = ± .35 K = 4.4.
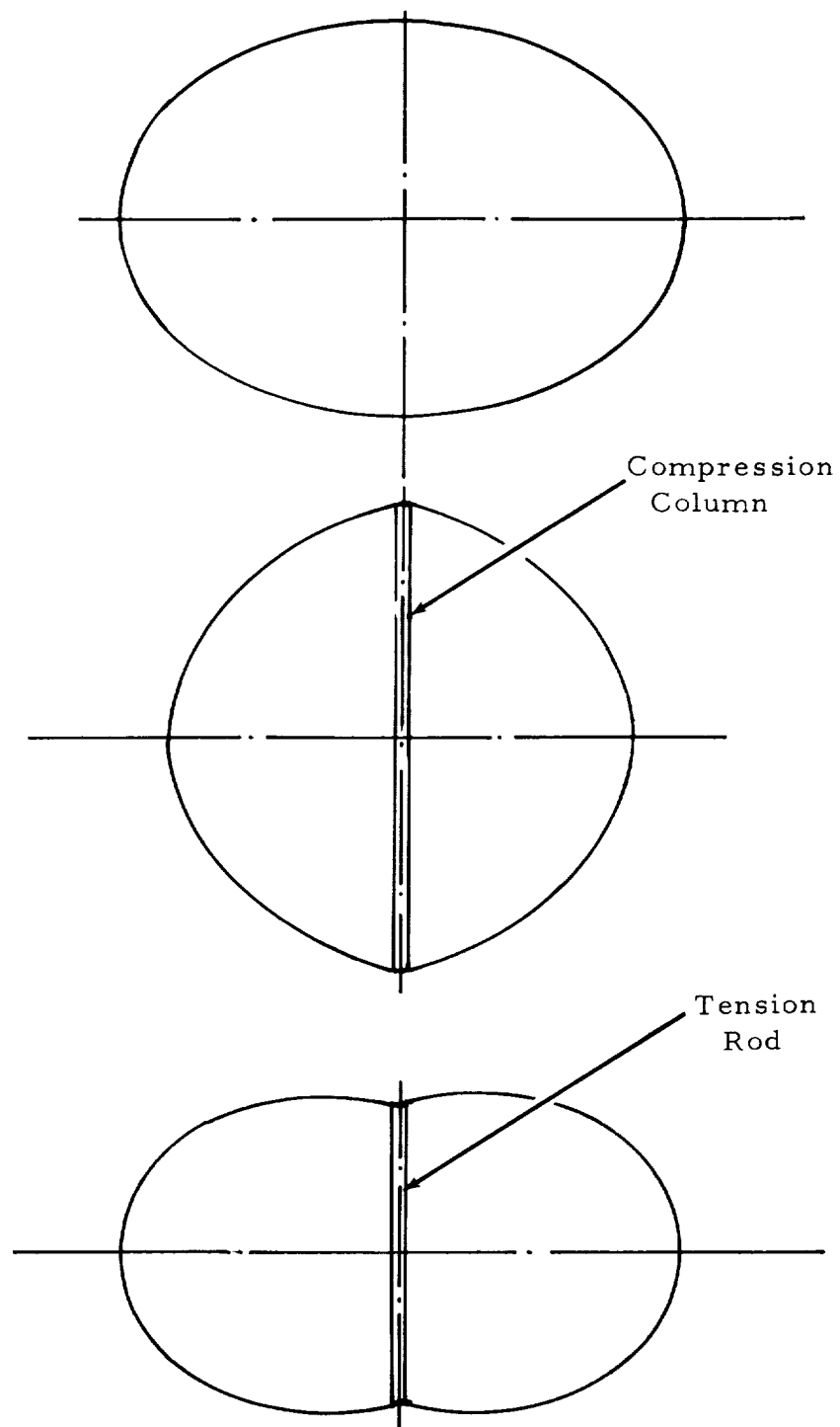
Figure 21.- Closed Isotensoid Pressure Vessel - Type I.
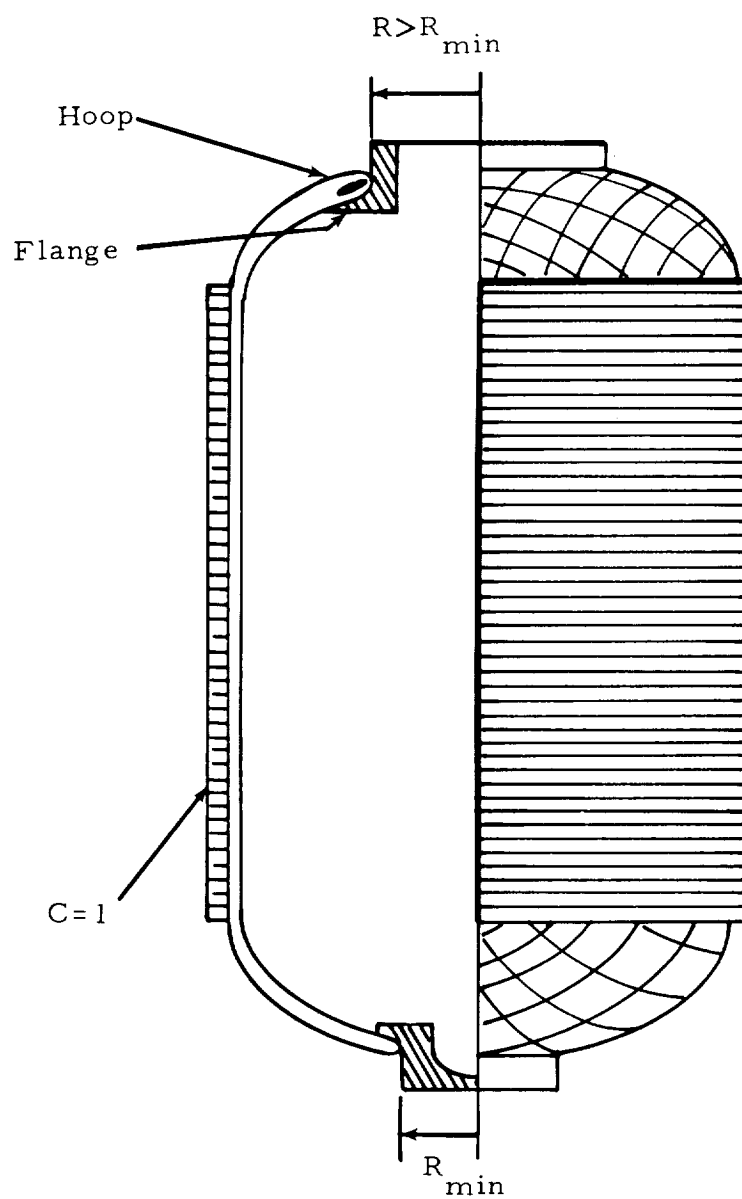
Figure 22. - Closed Isotensoid Pressure Vessel - Type II.

(a)

Hub

(b)

Hoop
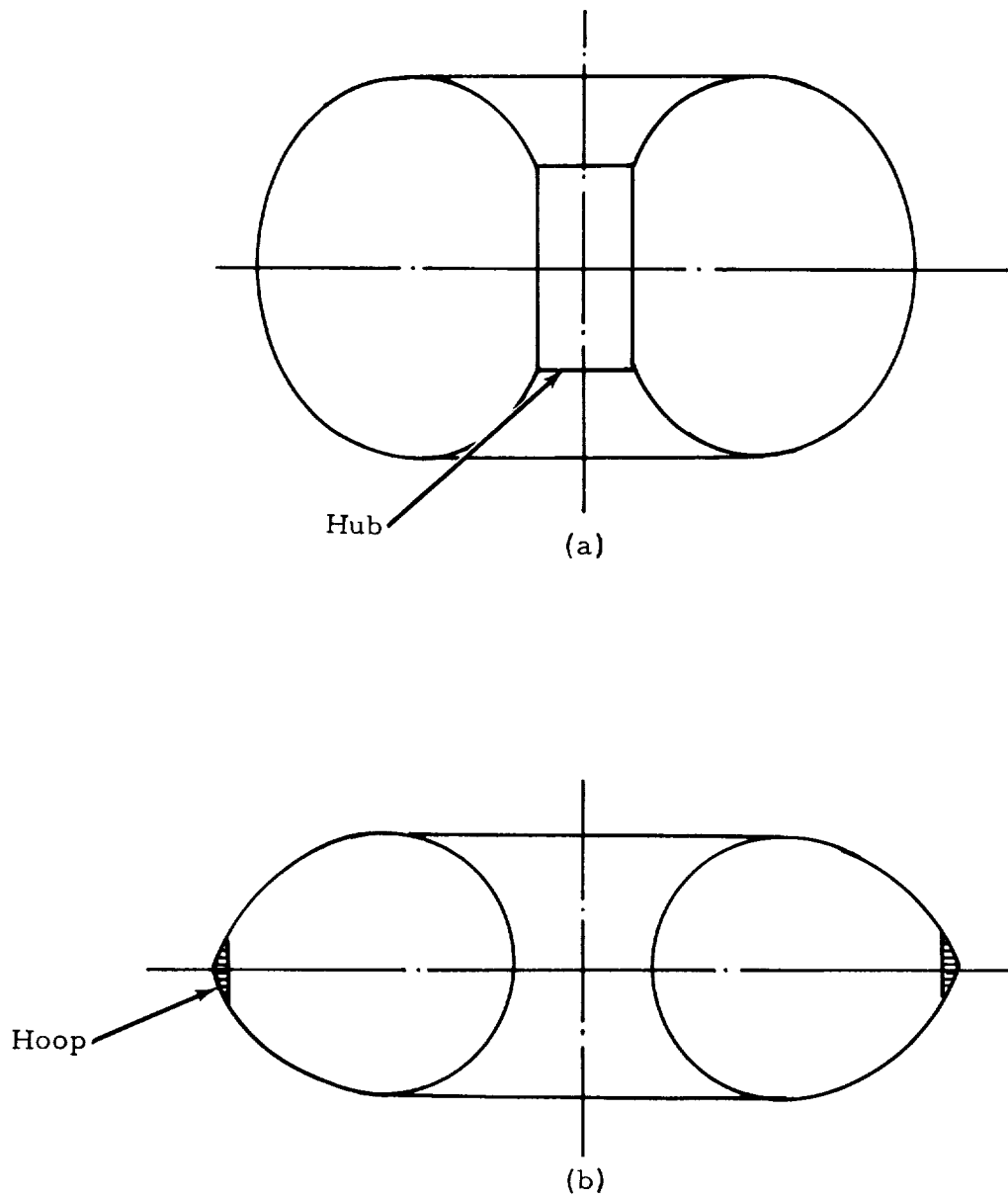
Figure 23. - Closed Isotensoid Pressure Vessel - Type III.
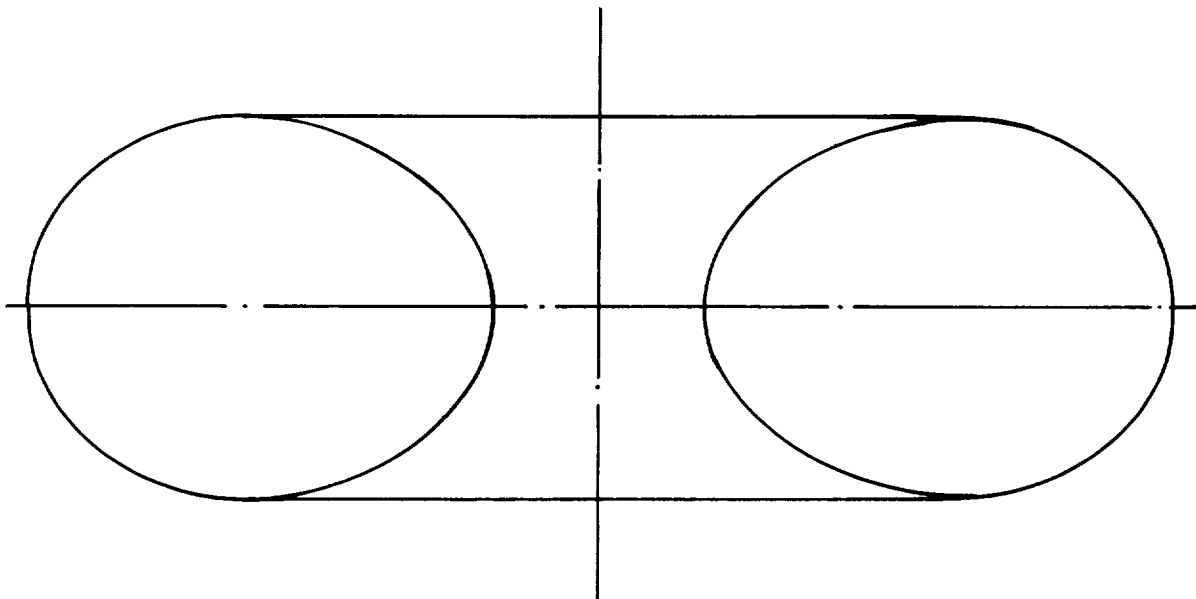
Figure 24.- Closed Isotensoid Pressure Vessel - Type IV.
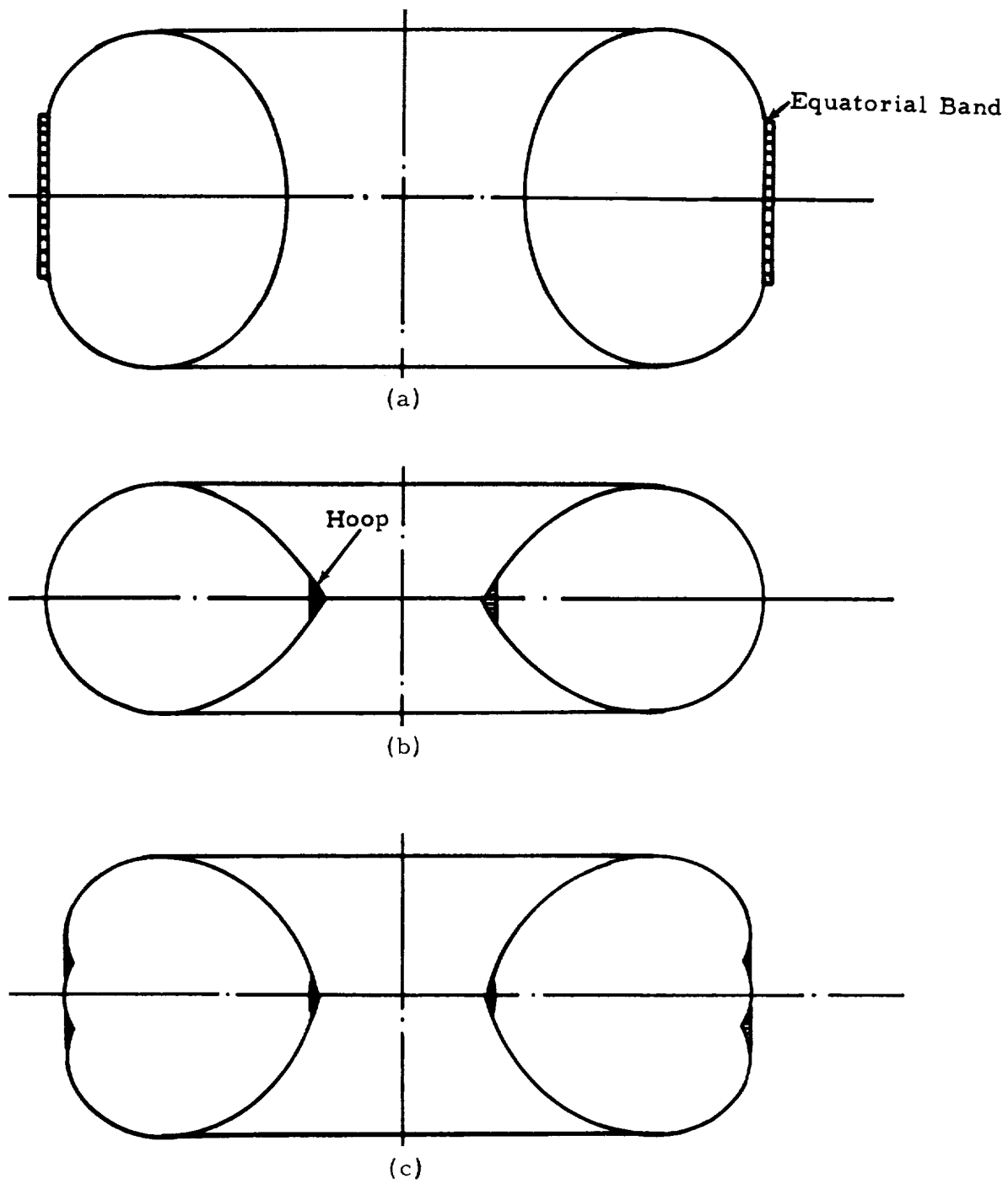
Figure 25. - Closed Isotensoid Pressure Vessel - Type V.
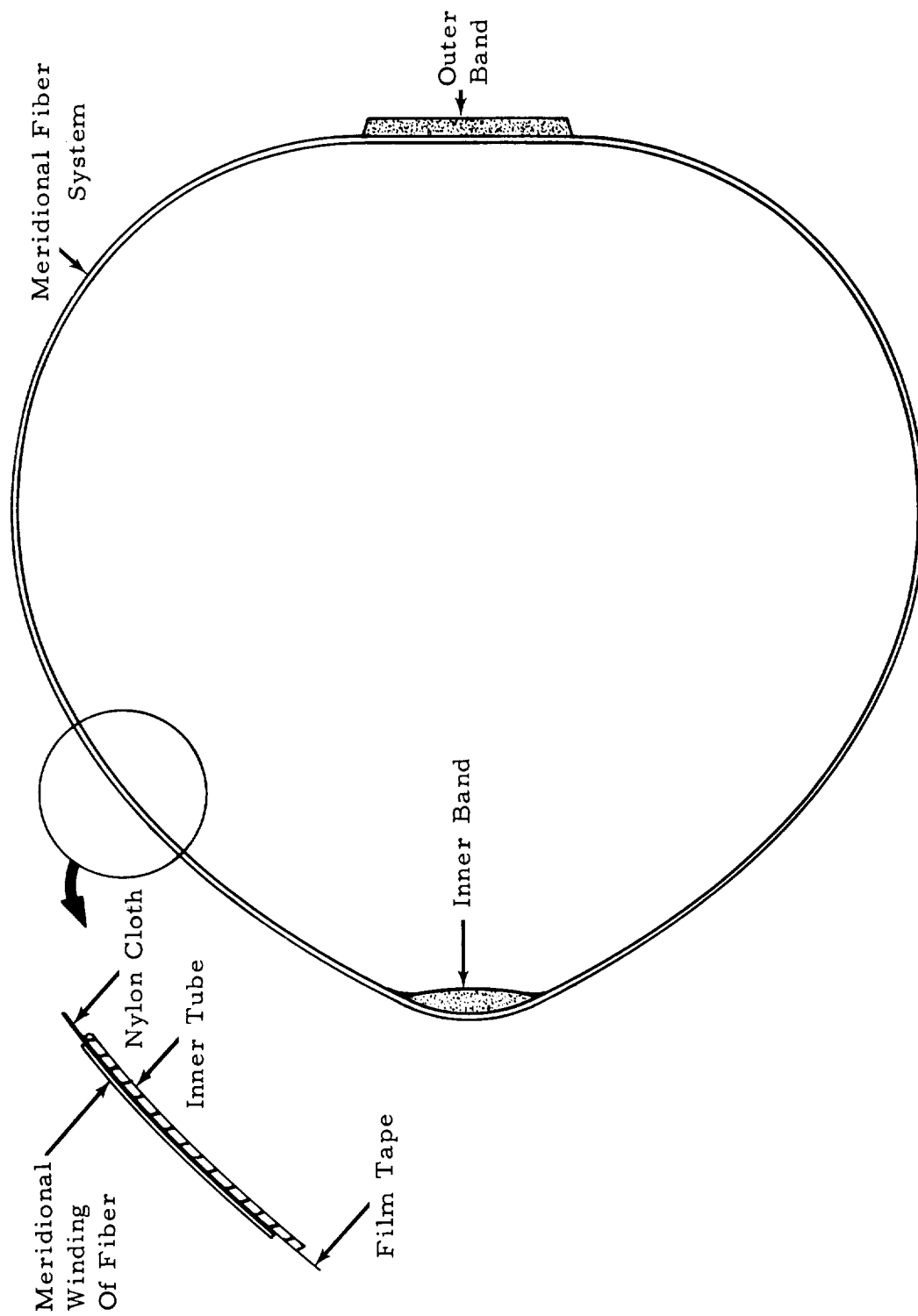
Figure 26. - Typical Cross Section, Meridionally-Wound Toroid.
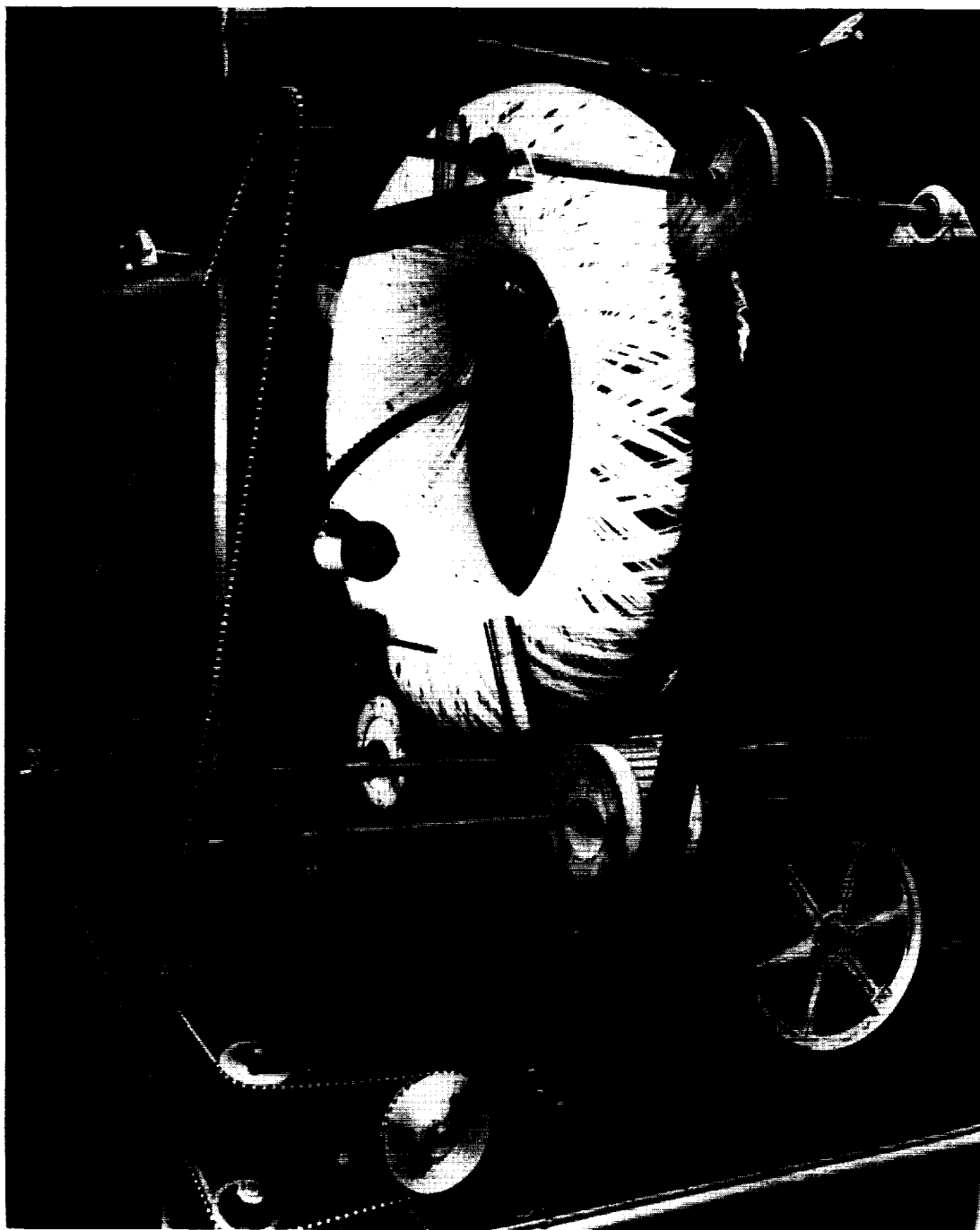
Figure 27. - Toroid Filament Winder.
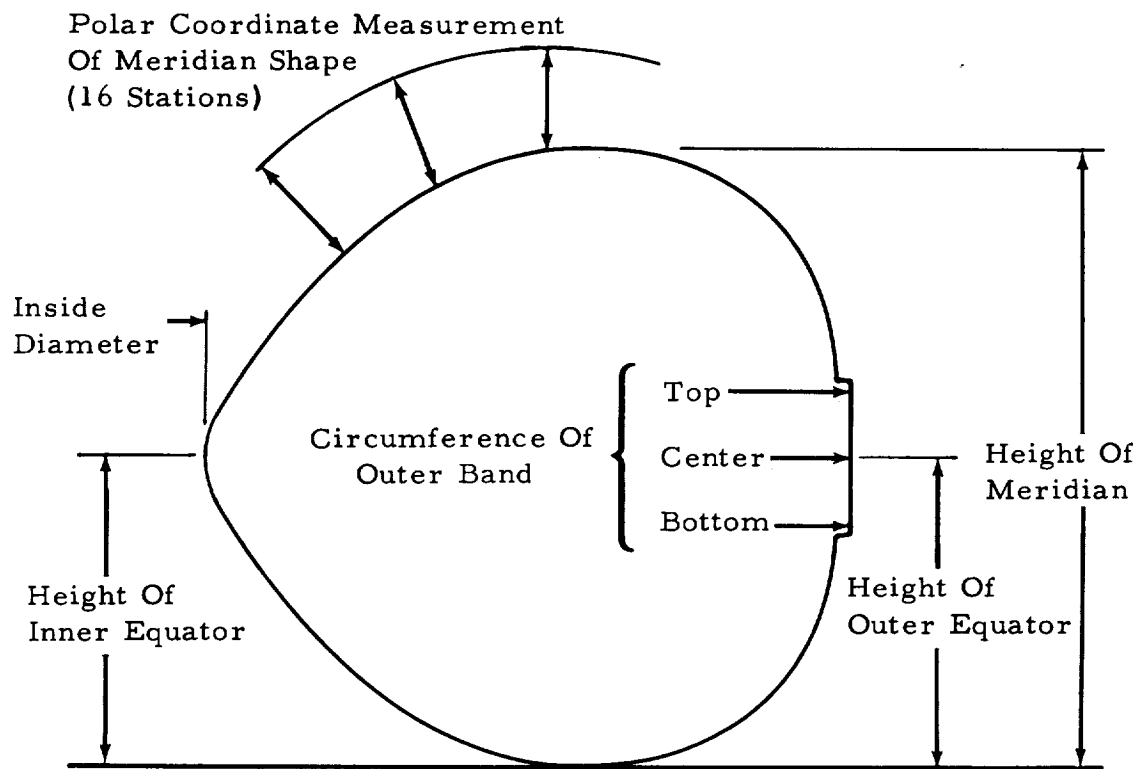
Figure 28. - Measurements Made on Toroid.

72
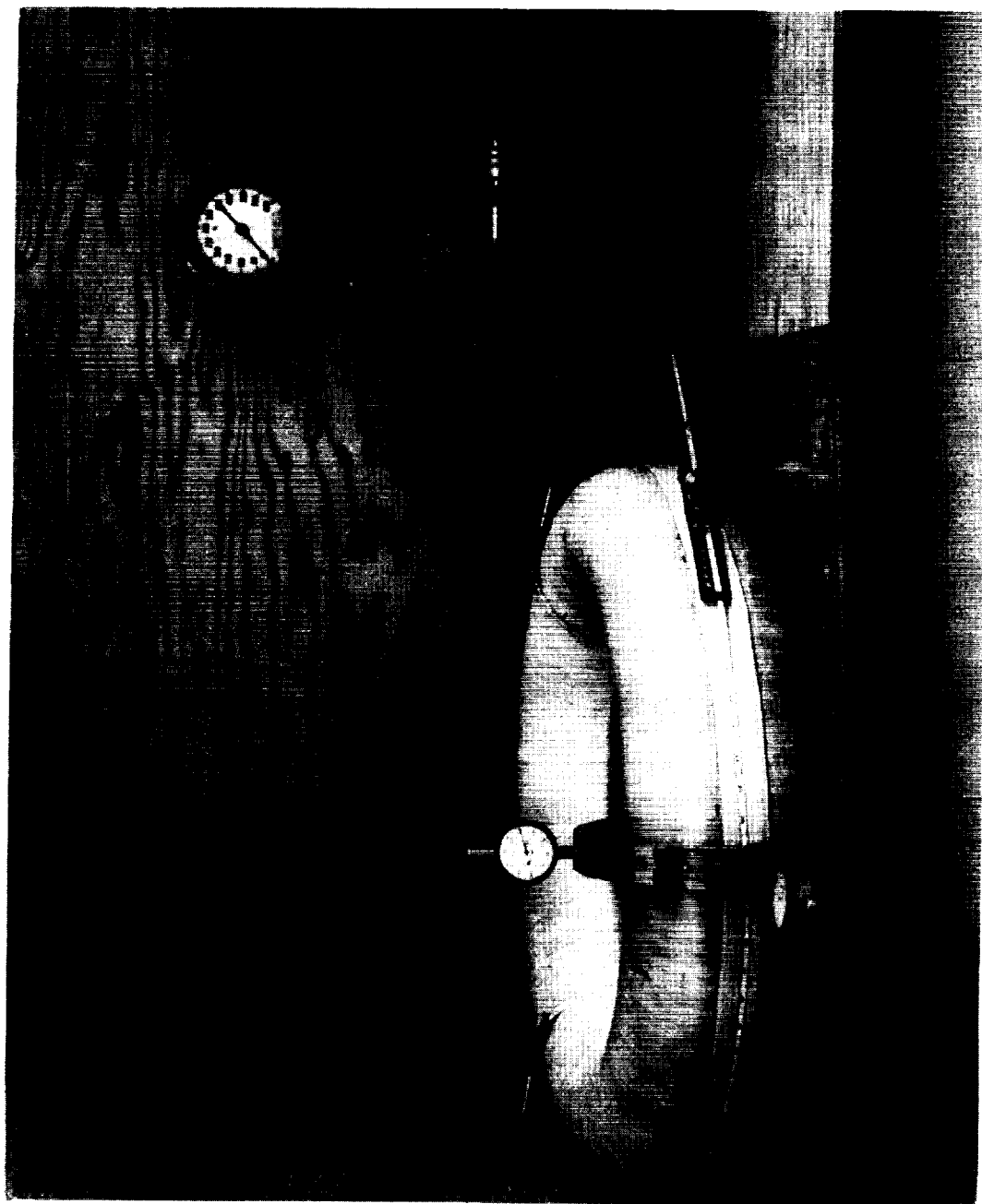
Figure 29. - Toroid Test Set-Up.
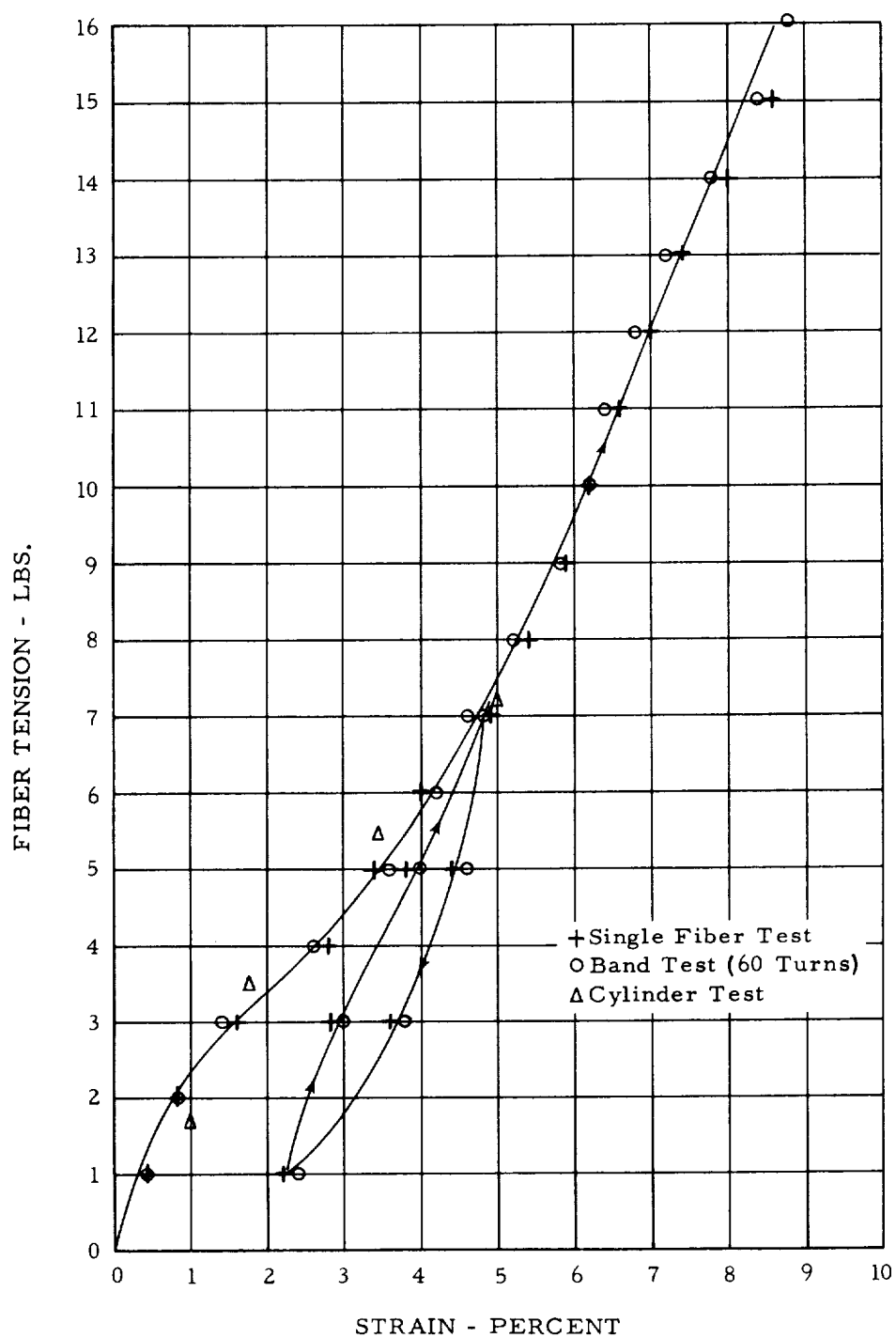
Figure 30. - Typical Load-Elongation Data For Polyester Fiber.

74
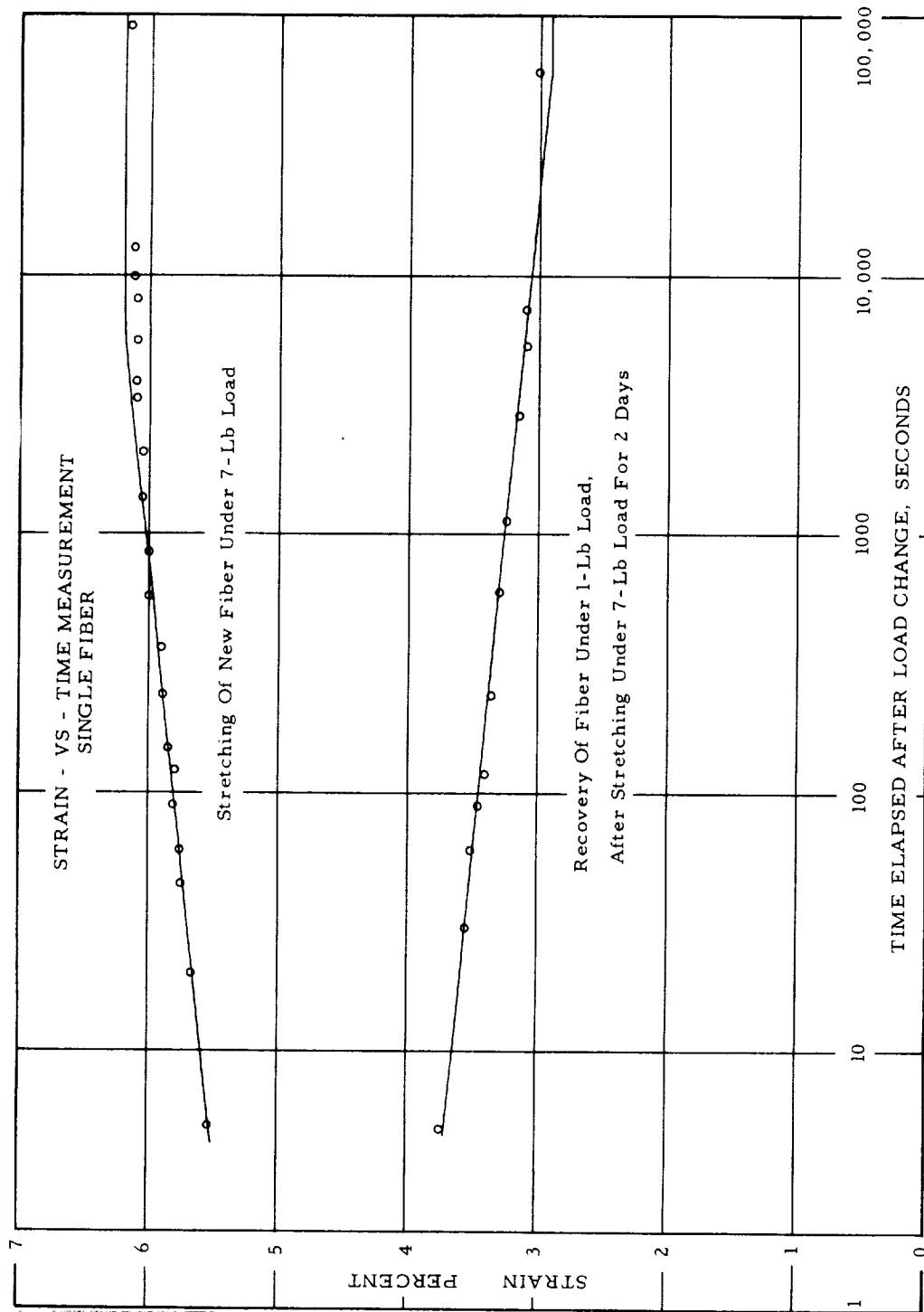
Figure 31. - Strain-Time Measurement For Single Fiber.
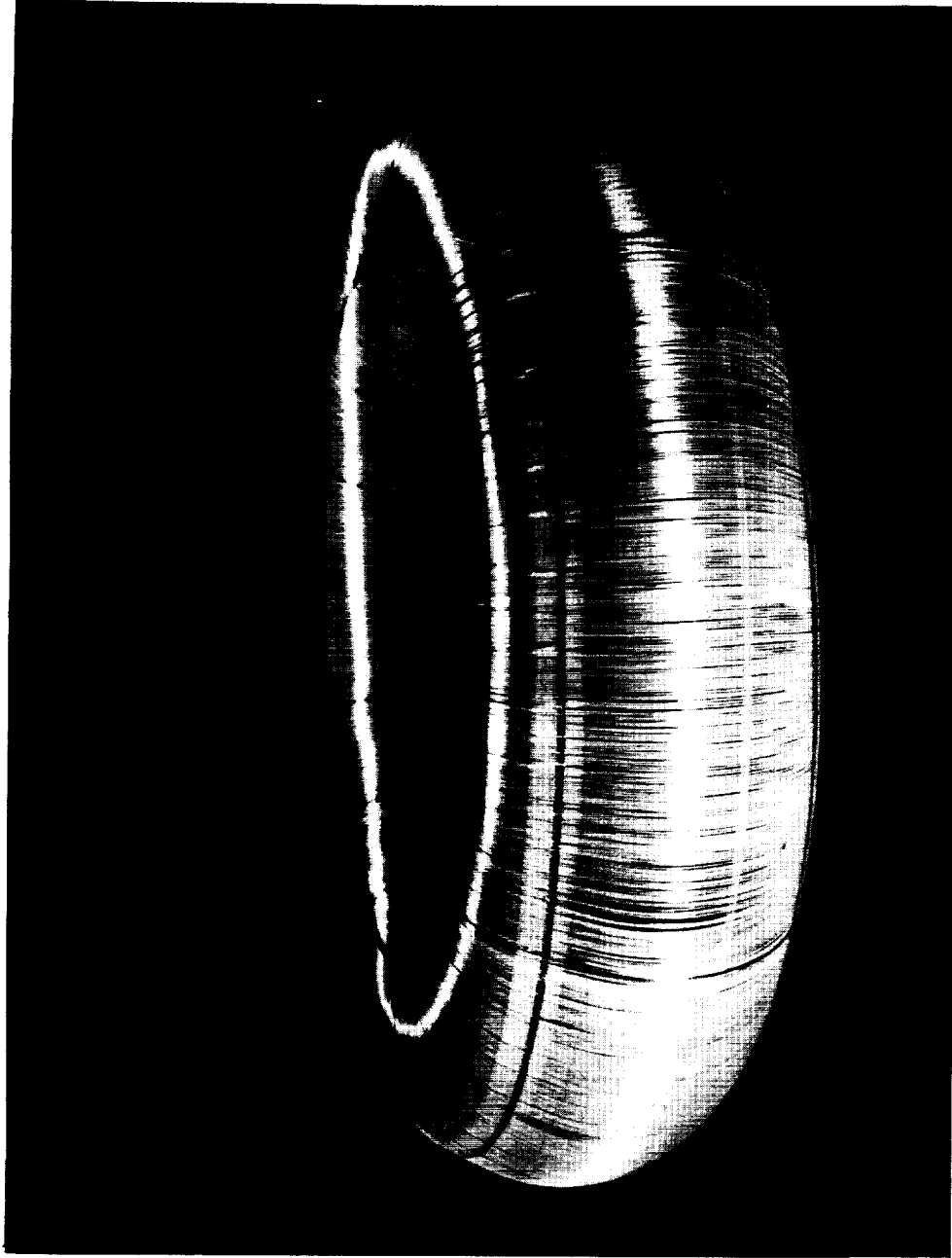
Figure 32. - "Rolling" Instability.
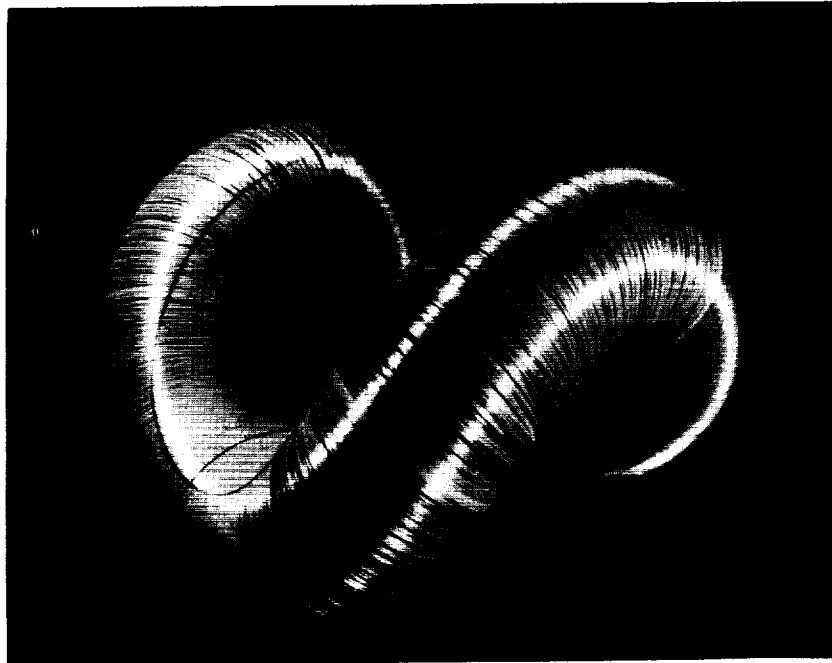
Figure 33. - Two-Lobed "Baseball Seam" Instability of Type V
Toroidal Isotensoid Pressure Vessel.
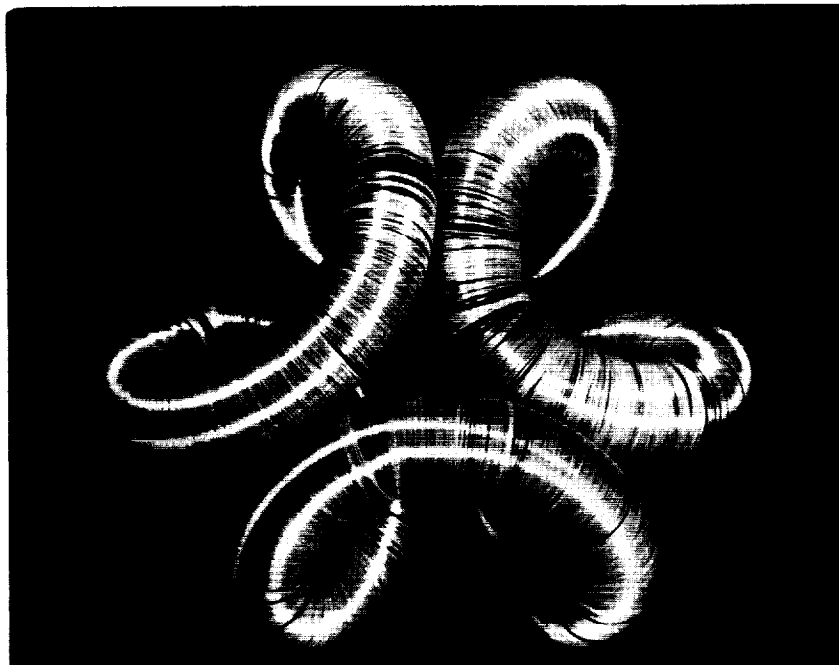
Figure 34. - Three-Lobed "Baseball Seam" Instability of Type V
Toroidal Isotensoid Pressure Vessel (Top View).
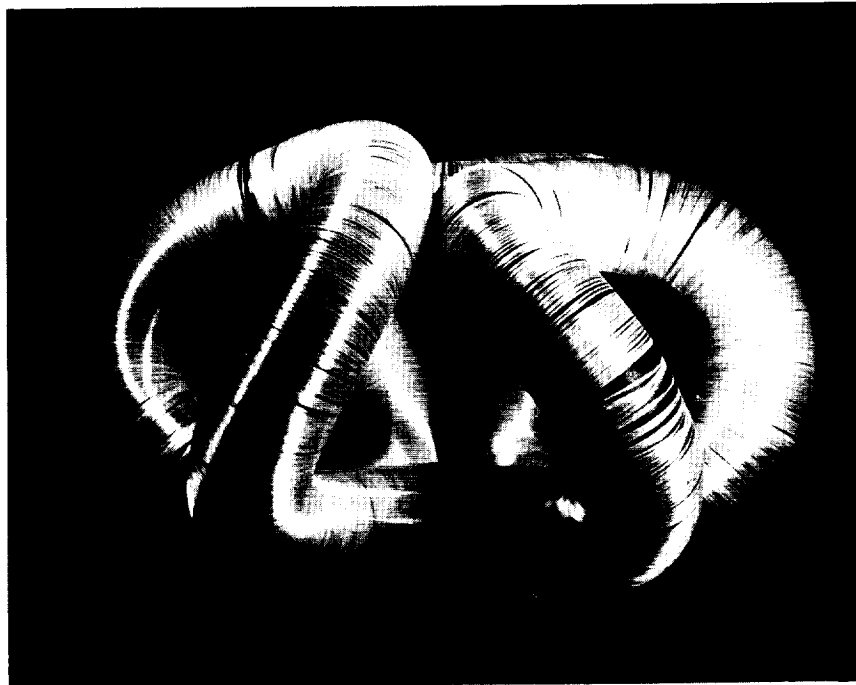
Figure 35. - Three-Lobed "Baseball Seam" Instability of Type V Toroidal Isotensoid Pressure Vessel (Side View).
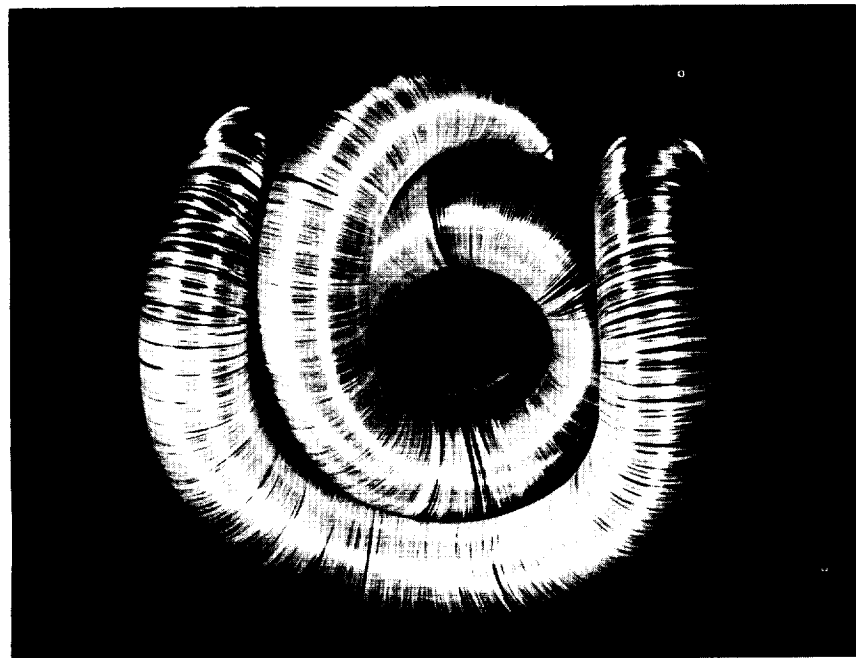
Figure 36. - "Python" Instability of Type V Toroidal Isotensoid Pressure Vessel.
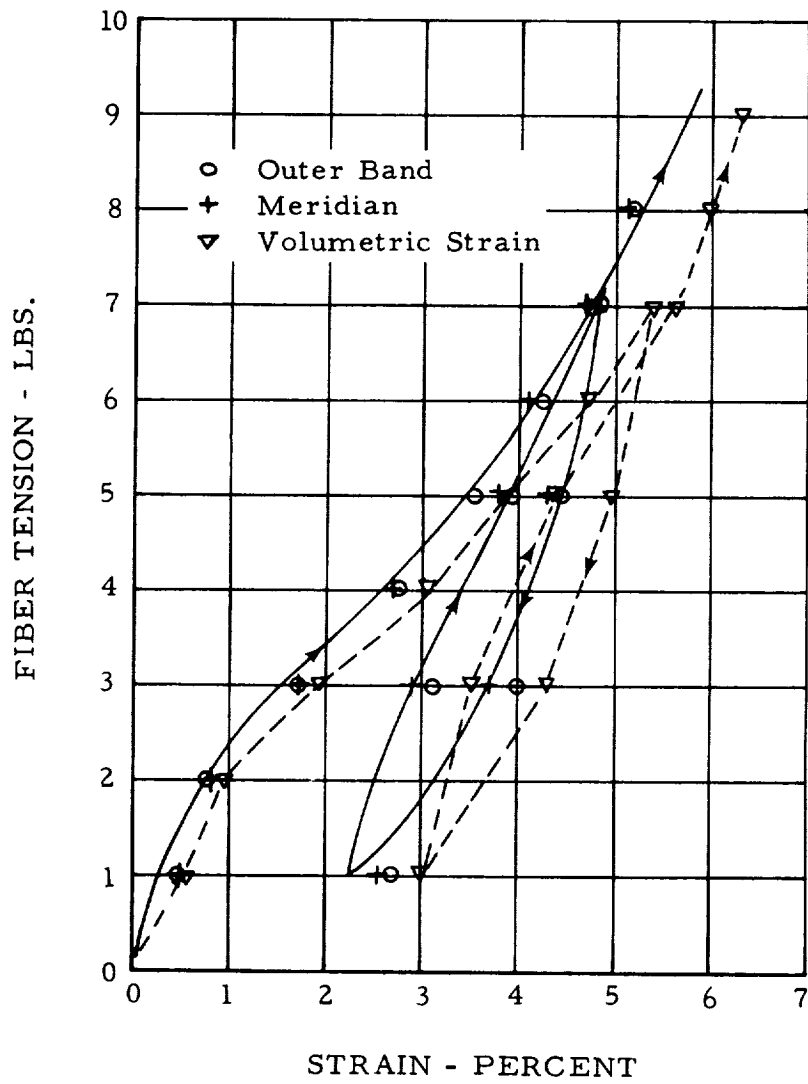
Figure 37. - Fiber Tension vs. Strain, Toroid #4.
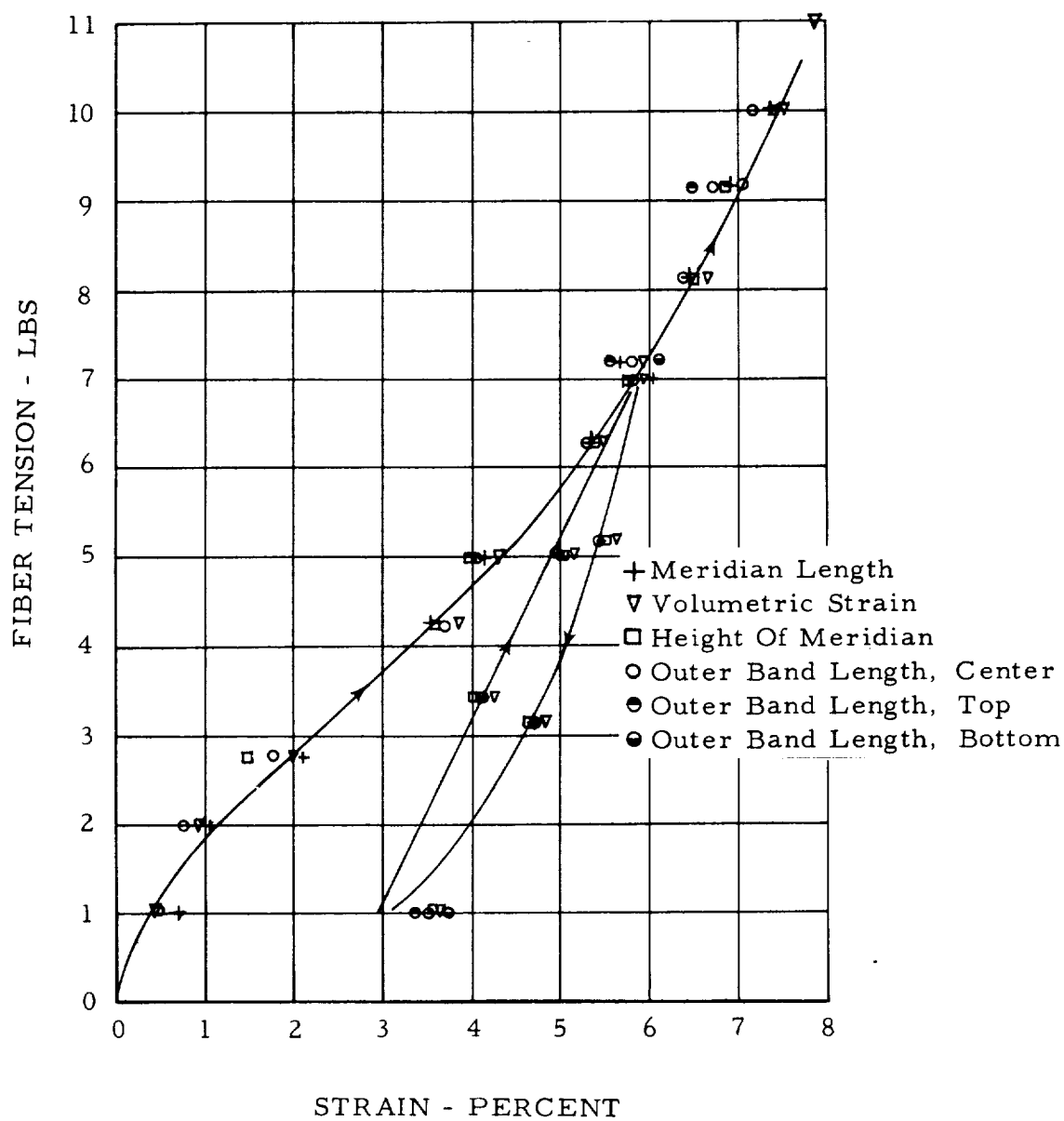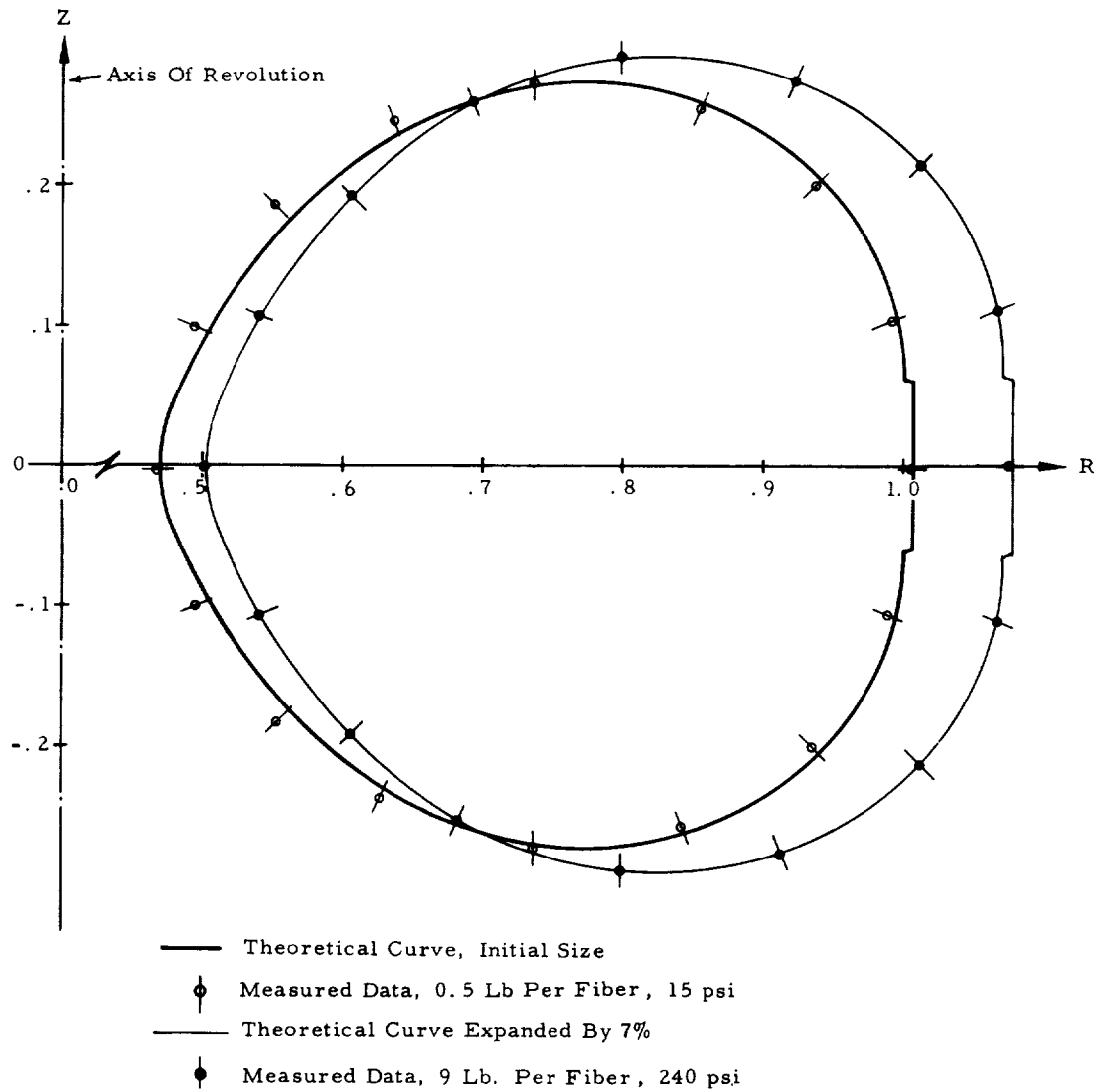
Figure 38. - Fiber Tension vs. Strain, Toroid #5.

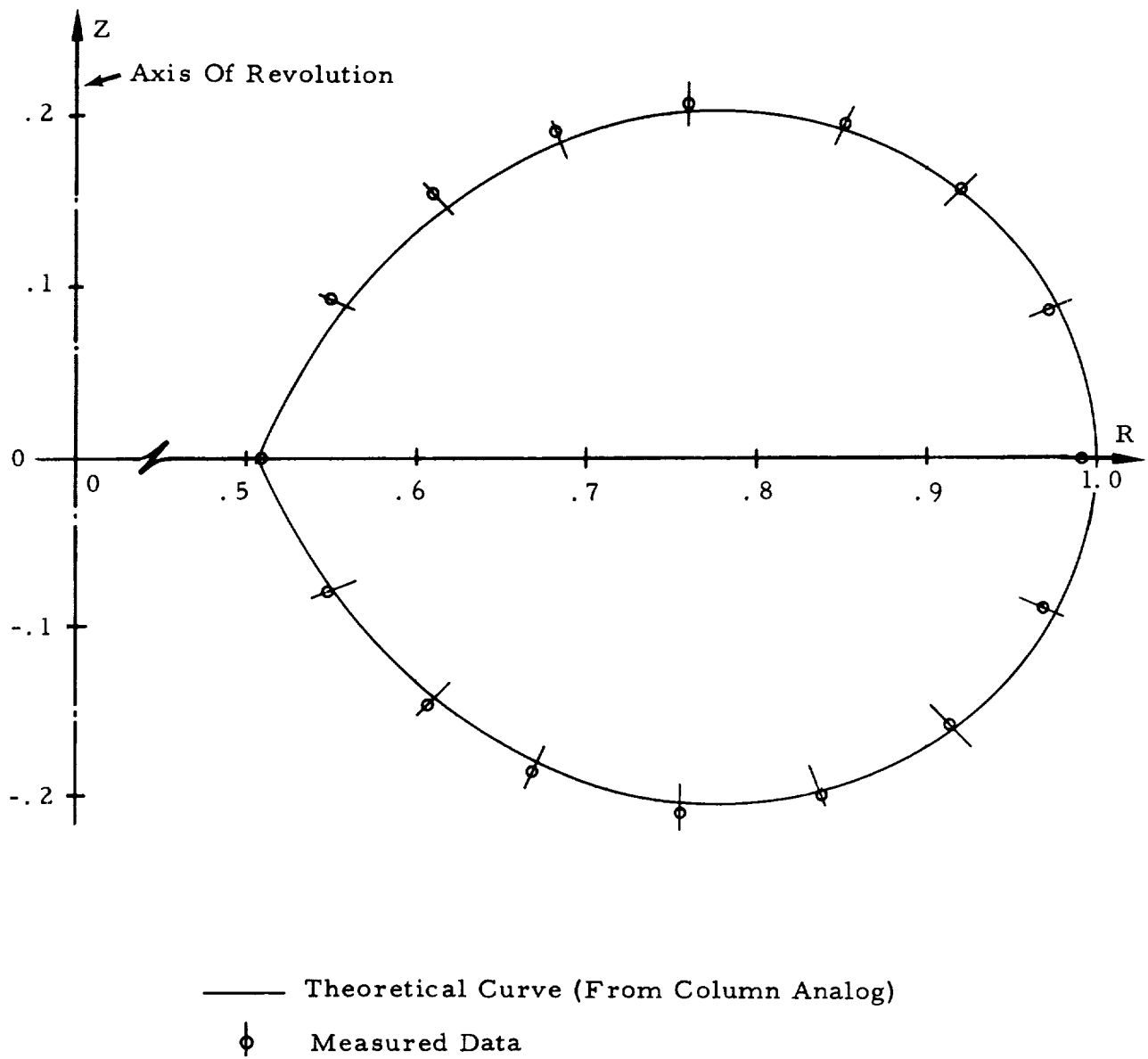Figure 39. - Cross-Section Measurement, Toroid #5.

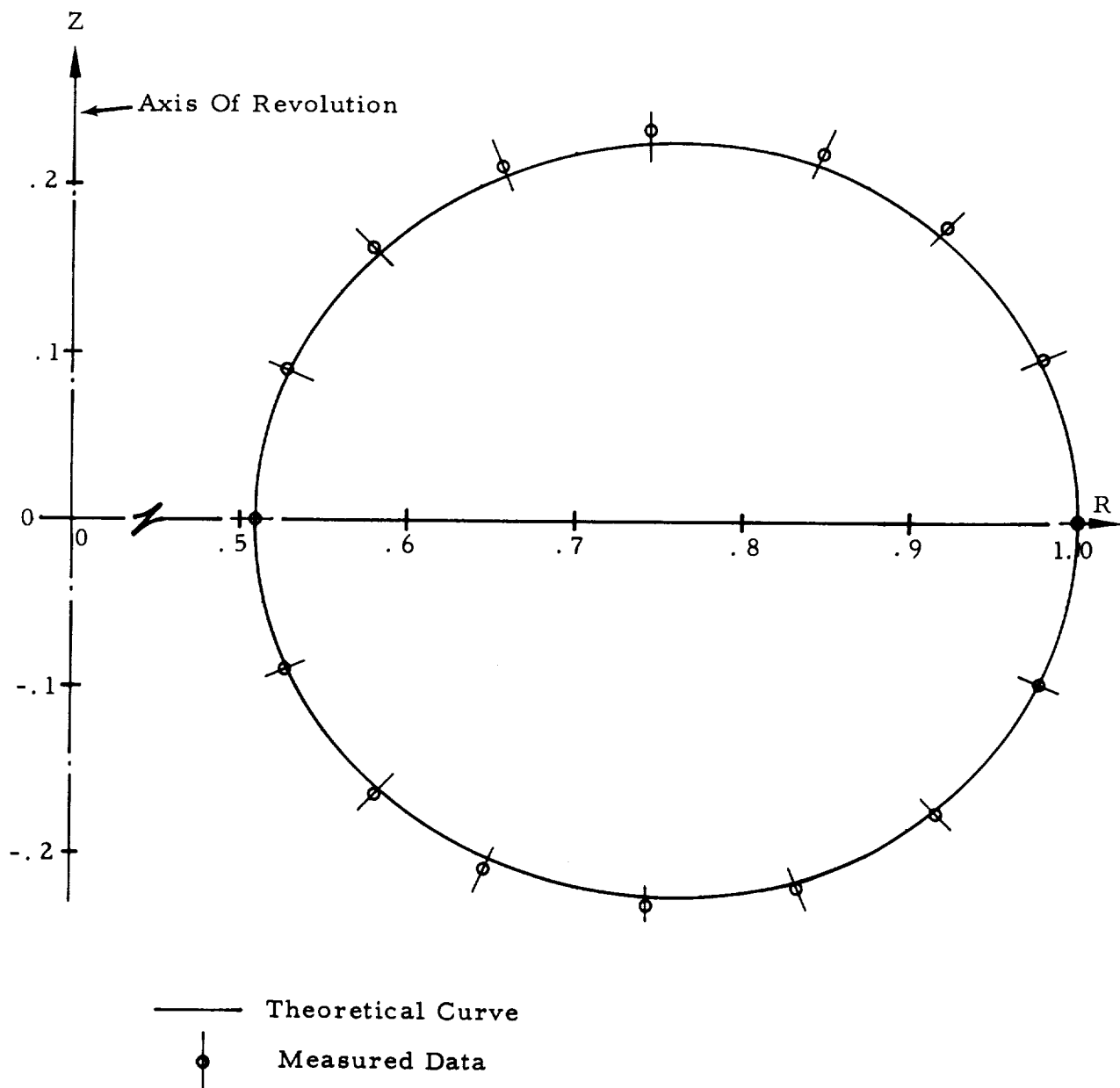Figure 40. - Toroid #3.

Figure 41. - Cross-Section Measurement, Toroid #3.

Figure 42. - Cross-Section Measurement, Toroid #6.